

# Latest Permian paleosols from Wapadsberg Pass, South Africa: Implications for Changhsingian climate

Robert A. Gastaldo<sup>1,†</sup>, Cassandra L. Knight<sup>1,†</sup>, Johann Neveling<sup>2,†</sup>, and Neil J. Tabor<sup>3,†</sup>

<sup>1</sup>Department of Geology, Colby College, Waterville, Maine 04901, USA

<sup>2</sup>Council for Geosciences, Private Bag x112, Silverton, Pretoria 0001, South Africa

<sup>3</sup>Huffington Department of Earth Sciences, Southern Methodist University, P.O. Box 750395, Dallas, Texas 75275-0395, USA

## ABSTRACT

Terrestrial settings preceding the end-Permian crisis are reported to trend toward increasingly dry and arid conditions, resulting in landscape change and a shift in fluvial architectures and regimes. Much of the latest Permian (Changhsingian) stratigraphic record in the Karoo Basin, South Africa, consists of paleosols, which record the physical conditions across time and space. Preboundary sequences at Wapadsberg Pass, Eastern Cape Province, provide insight into the climate regime that influenced paleosol formation at that time. A high-resolution sedimentological and geochemical study of two, stacked aggradational paleosols, in conjunction with stable isotope geochemical characterization of paleosol carbonate-cemented concretions over a 90 m section at this locality, demonstrates that these landscapes were predominantly wetland terrains without a demonstrable trend in increasing drying up to the Permian-Triassic boundary, as defined by vertebrates in the area.

Two paleosols examined 70 m below the Permian-Triassic boundary are identified as Protosols, and the former soil-air interface of each is marked by an autochthonous forest-floor litter in which canopy leaves of *Glossopteris* and groundcover plants of *Trizygia* are preserved. Molecular weathering ratios (e.g., base loss, clayeyness, chemical index of alteration minus potassium [CIA-K], etc.) determined from these horizons are indicative of immature soil development under water-saturated conditions. Assuming that paleosol-matrix concentrations of trace elements are indicative of Permian soil-solution chem-

istries, high concentrations of Ni, Cu, Ba, and Cr may have been growth-stress factors that may account for the small glossopterid leaf size in the megaflores, in contrast to current models that implicate stress in response to climate change.

Stable isotope  $\delta^{18}\text{O}$  and  $\delta^{13}\text{C}$  values are presented for micritic and microspar (<20  $\mu\text{m}$ ) calcite cements from carbonate nodules collected at 15 horizons through a 90 m stratigraphic interval up to, and including, the Permian-Triassic boundary. These isotopic ratios exhibit dissimilar trends. No clear trend exists in  $\delta^{18}\text{O}$  (Peedee belemnite [PDB] values range from  $-14.7\text{‰}$  to  $-21.8\text{‰}$ ). In contrast, a trend exists in  $\delta^{13}\text{C}$  values, where carbonate cements almost certainly precipitated under well-drained conditions in an interval that is 60 m below the Permian-Triassic boundary ( $-5.3\text{‰}$ ), while  $\delta^{13}\text{C}$  values as low as  $-16.9\text{‰}$ , indicative of water-logged conditions, begin 90 m below and continue up to the Permian-Triassic boundary. Hence, no evidence is found for a preboundary trend toward increasing aridity at this locality. The first estimates of the latest Permian atmospheric  $p\text{CO}_2$  from paleosols, based on coexisting calcite and organic matter  $\delta^{13}\text{C}$  values from paleosols that developed under well-drained conditions, provide a range of values from 900 to 1900, and 500 to 1300 ppmV, respectively, which are significantly lower than the latest Early Permian, when terrestrial biome replacement is documented to have occurred.

## INTRODUCTION

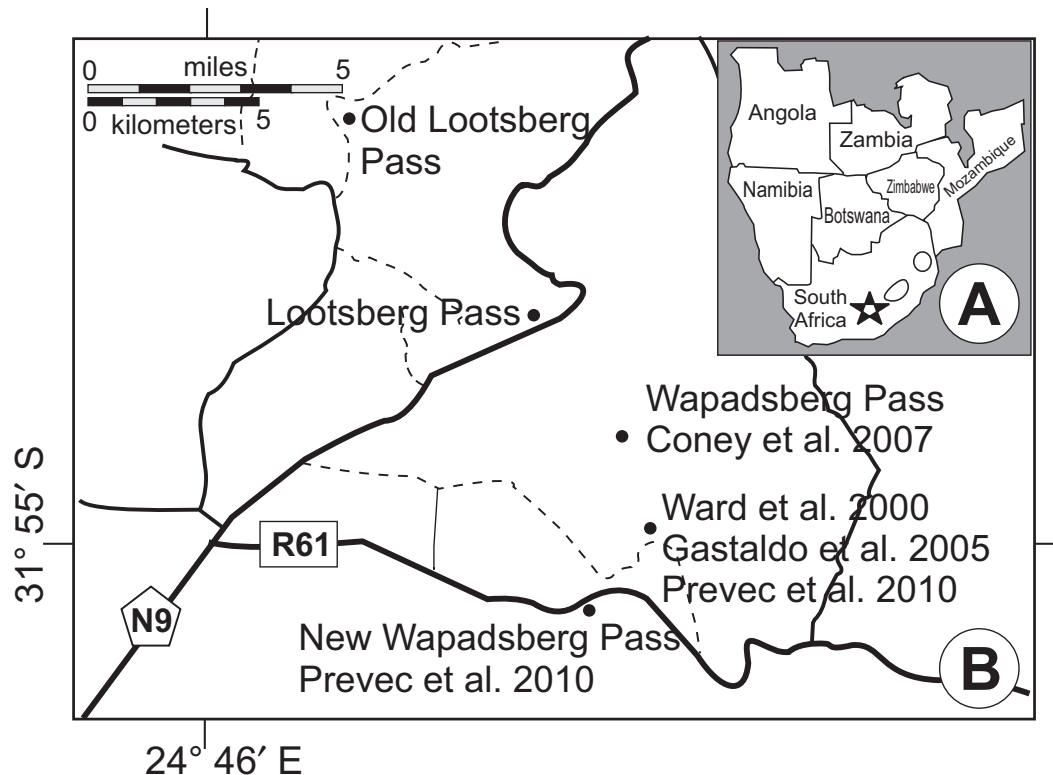
The rapid Permian-Triassic extinction event, the zenith of which is constrained over a 200 k.y. interval ( $252.28 \pm 0.08$ – $252.10 \pm 0.06$  Ma; Shen et al., 2011), is well documented in the marine realm, with estimates of biodiversity loss at the generic level ranging from nearly 75% to 100%

(Payne and Clapham, 2012). In contrast, terrestrial biodiversity loss is reported either to be asynchronous (Xiong and Wang, 2011) or synchronous (e.g., Twitchett et al., 2001; Smith and Ward, 2001; Ward et al., 2005; Shen et al., 2011) with the marine event, but the quality of the continental paleontological record may be more a function of taphonomic processes operating in conjunction with landscape dynamics (Gastaldo et al., 2005; Gastaldo and Demko, 2010). In the Karoo Basin, South Africa, the loss of  $\sim 82\%$  of terrestrial vertebrate taxa has been interpreted to be in response to Late Permian climatic drying, triggering vegetation and ecosystem collapse, followed by a shift in fluvial regimes to a braided configuration (Ward et al., 2000, 2005; Smith and Ward, 2001). The Permian-Triassic boundary is thought to be represented by the last appearance datum (LAD) of *Dicynodon lacerticeps*, supplemented with a small, negative stable carbon isotope excursion (e.g., Ward et al., 2005).

The biostratigraphically defined Permian-Triassic boundary in the Karoo Basin is exposed at only a few places in the Eastern Cape Province (Fig. 1; Old Lootsberg Pass, Tweefontein, Lootsberg Pass, Wapadsberg Pass, Carlton Heights—Ward et al., 2000, 2005; Retallack et al., 2003; Commandodrift Dam—DeKock and Kirschvink, 2004; Ward et al., 2005; Coney et al., 2007) and the Free State (Bethulie, Caledon—Smith, 1995; MacLeod et al., 2000; Ward et al., 2000; Smith and Ward, 2001). The stratigraphic position of the vertebrate extinction and a reported transition in fluvial styles, in what has been considered a continuous stratigraphic record, were believed to be associated with a “unique” boundary facies described from the Bethulie area (Ward et al., 2000; Retallack et al., 2003). This interval was reported as regionally correlative across the basin (Ward et al., 2005; Smith and Botha, 2005; Botha and Smith, 2006, 2007) and recognized elsewhere (Australia, Antarctica; Retallack et al., 2003).

<sup>†</sup>E-mails: ragastal@colby.edu (Gastaldo, corresponding); knight.cassi@gmail.com (Knight); jneveling@geoscience.org.za (Neveling); ntabor@smu.edu (Tabor).

**Figure 1.** Geographic location of Wapadsberg Pass localities, Eastern Cape Province, South Africa. (A) Map of southern Africa on which the generalized location is marked with a star. (B) Road map of the Eastern Cape Province on which the reported global positioning system (GPS) coordinates are plotted for: New Wapadsberg Pass along the R61 motorway (Prevec et al., 2010); Old Wapadsberg Pass (dashed line; Ward et al., 2000; Gastaldo et al., 2005; Prevec et al., 2010); Wapadsberg Pass (Coney et al., 2007); and Lootsberg Pass (Ward et al., 2000, 2005; Retallack et al., 2003; Gastaldo et al., 2009), for reference.



Recently, Gastaldo et al. (2009) and Gastaldo and Neveling (2012) demonstrated that this “laminite bed,” or “dead zone,” used by all previous authors both to identify, and as the datum by which to correlate, the Permian-Triassic boundary and biotic crisis, is neither correlative nor does it occur at the same stratigraphic position in Bethulie (*sensu lato*) and Lootsberg Pass, two critical cornerstones in the extinction model. Hence, because each locality exhibits a unique stratigraphic record, and the Permian-Triassic boundary is known to have been lost through erosion elsewhere in the basin (Hancox et al., 2002), it is necessary to evaluate the stratigraphy in each reported locality to document the changes in landscape leading to the LAD of *Dicynodon lacerticeps* (Kammerer et al., 2011).

The Permian-Triassic transition at Wapadsberg Pass is exposed in two areas, where both fluvial channel and paleosol sequences occur. The first is in an erosional gully (*donga*) west of a dirt road that served as the principal mountain pass until construction of the R61 Highway, whereas the second outcrops adjacent to the R61 Highway >1.5 km to the southwest (Fig. 1). A 90+ m stratigraphic section at Old Wapadsberg Pass includes the vertebrate-defined Permian-Triassic boundary (Ward et al., 2000; Coney et al., 2007), and it exposes thick siltstones in which carbonate-cemented siderite nodules are common. In addition, an autochthonous,

*Glossopteris*-rich forest litter is reported from ~70 below the reported boundary (Prevec et al., 2010) that is correlated to the R61 section, where the best preserved material occurs above aggradational (intervals of net deposition and increasing elevation in floodplains adjacent to river systems; Bull, 1991) paleosols. The forest litter is characterized by a low-diversity flora with small-leaved glossopterid (gymnosperm) canopy detritus along with sphenophyll (equisetalean) groundcover in which an array of invertebrates is preserved. The recovered palynological assemblage is assigned a late Changhsingian age (Prevec et al., 2010; Fig. 2), with several Early Triassic forms present, including *Falcisporites australis* reported as the pollen of a characteristic Early Triassic peltasperm taxon in Australia (Retallack, 2002). Siltstone intervals both below and above the fossil flora also contain calcareous nodules.

The goal of the current contribution is twofold. The first is to characterize and determine the geochemical trends of two aggradational, rooted paleosols exposed along the R61 Highway cut (Prevec et al., 2010) as a baseline for latest Changhsingian, preboundary landscape conditions. The second is to evaluate the trends in stable isotope geochemistry recorded in the sequence of carbonate-cemented nodules beginning 90 m below, and ending at the end-Permian paleosol (DeKock and Kirschvink, 2004) to

test the hypothesis of an overall trend in aridification. While these data cannot help constrain the current placement of the vertebrate-defined Permian-Triassic boundary at Wapadsberg Pass, they may clarify the interpretations of environmental conditions prior to the reported extinction event.

#### Karoo Whole-Rock Geochemistry

To date, limited numbers of geochemical studies are reported from the Karoo Basin. These are focused on basinwide, paleoenvironmental conditions following deglaciation (Scheffler et al., 2003, 2005) and leading up to, and across, the biostratigraphically defined Permian-Triassic boundary (Maruoka et al., 2003; Coney et al., 2007). A shift from a humid, warm Early Permian climate to increasingly arid, warm Middle Permian conditions was interpreted by Scheffler et al. (2005) based on the stratigraphic trends of weathering proxies including chemical index of alteration (CIA), Zr/Ti, Rb/K, and V/Cr ratios, and total organic carbon (TOC) values. Warm, seasonally arid conditions are conceived to persist into the latest Permian based, in part, on stable isotopic values from carbonate-cemented concretions (Ward et al., 2000, 2005). However, no other evidence has been found to indicate any geochemical proxy change or trend associated with the boundary event (DeWit

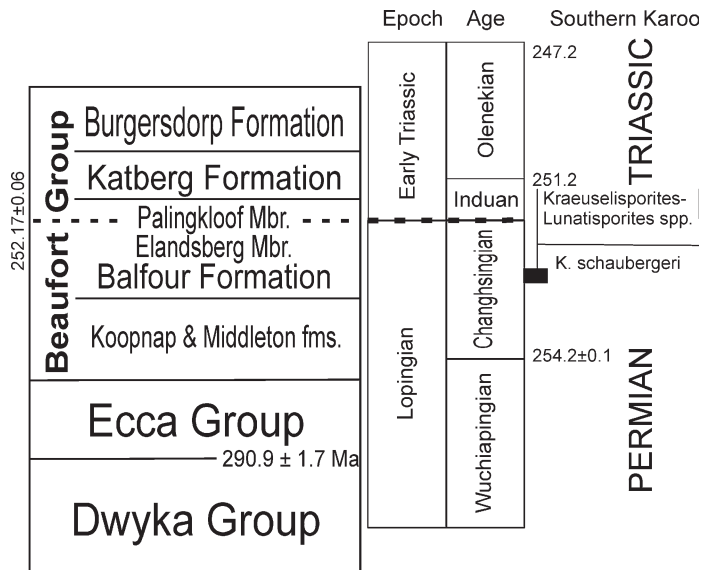


**Figure 2.** Generalized stratigraphy of the Karoo Basin, South Africa, illustrating the stratigraphic position of formations and members discussed herein. Biostratigraphic and age assignments (in Ma) of Wapadsberg Pass plant-fossil assemblage are based on palynology (Prevec et al., 2010); chronometric age for the Permian-Triassic boundary is from Shen et al. (2011); the Dwyka-Ecca boundary age is from Stollhofen et al. (2008), and dates for Epoch/Stage boundaries are based on the International Chronostratigraphic Chart of the International Commission on Stratigraphy, Permian Time Scale, 2012 version.

Permian-Triassic boundary rocks in the basin (Ward et al., 2000; Smith and Botha, 2005; Botha and Smith, 2006), except for those of Retallack et al. (2003), who defined a suite of immature and poorly developed to mature and well-developed Permian and Triassic paleosol types. This latter scheme is considered ambiguous (see supplemental data Table DR1<sup>1</sup>), and the paleosol-specific classification of Mack et al. (1993) is favored in the current study.

## MATERIALS AND METHODS

The stratigraphic interval in which the stacked paleosols reported by Prevec et al. (2010) occur is ~70 m below the biostratigraphically defined Permian-Triassic boundary (Ward et al., 2005), and it crops out in the road cut along the R61 Highway at New Wapadsberg Pass (31°55.927'S, 24°52.872'E) and >1.5 km to the northwest of the road cut in two dongas beneath Old Wapadsberg Pass (31°55.199'S, 24°53.666'E; 31°55.108'S, 24°53.692'E; Fig. 1). The presence of vertically to subvertically oriented fossil woody (open-cylinder-type *Vertebraria*) and nonwoody roots, rhizoconcretions, and/or horizons of calcite-cemented nodules was used to delimit paleosols (Figs. 3 and 4). In addition, the preservation of forest-floor litter on two, closely spaced bedding surfaces allowed for the recognition of an aggradational sequence based on the occurrence of these interpreted organic (O) horizons (Prevec et al., 2010; Fig. 5). High-resolution (centimeter-scale) stratigraphic sections were measured in the current study using a Jacob's staff with site level and standard field and descriptive methods. A photomosaic of the R61 road cut was constructed, allowing for identification of large-scale features above and below the paleosol interval.

Outcrop trenching was used to recover minimally weathered hand samples in both New Wapadsberg Pass and Old Wapadsberg Pass sites. Samples for thin sections and geochemical analyses were taken from a white claystone (tuffite) overlying the fossil-plant horizon, the preserved leaf-litter horizon, and at 10 cm intervals below each O-horizon at separate localities to a depth of 70 cm. Where a stratigraphic horizon was found to be iron-stained, hand samples for geochemical analysis were vetted to eliminate excess contamination by precipitated secondary mineralization. Samples from the Old

<sup>1</sup>GSA Data Repository item 2014060, measured stratigraphic sections at Wapadsberg Pass; comparative table of latest Permian paleosols; trace-element data tables and calculated soil molecular weathering ratios, is available at <http://www.geosociety.org/pubs/ft2014.htm> or by request to [editing@geosociety.org](mailto:editing@geosociety.org).

et al., 2002; Scheffler et al., 2005; Coney et al., 2007), and the presence of carbonate nodular horizons at different stratigraphic levels near the vertebrate-defined Permian-Triassic boundary is reported as evidence for spatial and temporal variation in paleoenvironmental settings (Coney et al., 2007). In contrast, Tabor et al. (2007) used coexisting calcite and organic matter from Karoo paleosols to demonstrate that nodule genesis is either (1) a response to closed-system conversion of organic matter to calcite under waterlogged soil conditions (possibly through methanogenesis), or (2) the result of carbonate precipitation under open-system diffusion of CO<sub>2</sub> and mixing with atmospheric CO<sub>2</sub> under evaporative soil processes.

## Karoo Permian Paleosols

A clear, comprehensive description of Karoo Basin paleosols has not heretofore been developed, nor is there agreement amongst authors about paleosol descriptions or classification schemes (Smith, 1995; Retallack et al., 2003; Smith and Botha, 2005; Botha and Smith, 2006, 2007; Tabor et al., 2007; Bordy et al., 2011). Smith's (1995) Late Permian (*Dicynodon* assemblage zone [AZ]; Rubidge, 1995) and Early Triassic (*Lystrosaurus* AZ) paleo-

sols are described in the context of interpreted landscapes, spatially related to coeval channel deposits. Three Permian paleosol types are placed in this landscape framework. Immature, Protosol-type (Mack et al., 1993) paleosols: are interpreted to have formed on channel banks and levees; are recognized by their greenish color; and may exhibit vertical calcareous tubules, rhizoconcretions, and small (<10 cm diameter), isolated calcareous nodules. More mature proximal floodplain paleosols are characterized by a maroon (grayish red), clay-enriched horizon, slickensides, and coalesced calcareous nodules (= Vertisol of Mack et al., 1993; Caudill et al., 1996). Distal floodplain settings record the most common paleosol, which is a greenish, hydromorphic Gleysol (Mack et al., 1993) in which extensive mottling (maroon or purple and greenish gray [olive gray]) is associated with root traces. Gypsum rosettes and septarian nodules may be present but are locally restricted where encountered. Permian paleosols are replaced by a single Triassic type (Smith, 1995). These are described as rubified, with green mottling confined to zones around rhizoconcretions, and they may exhibit desiccation cracks, well-developed calcitic horizons, or calcareous nodules. This landscape-paleosol model has been applied to subsequent stratigraphic descriptions of the

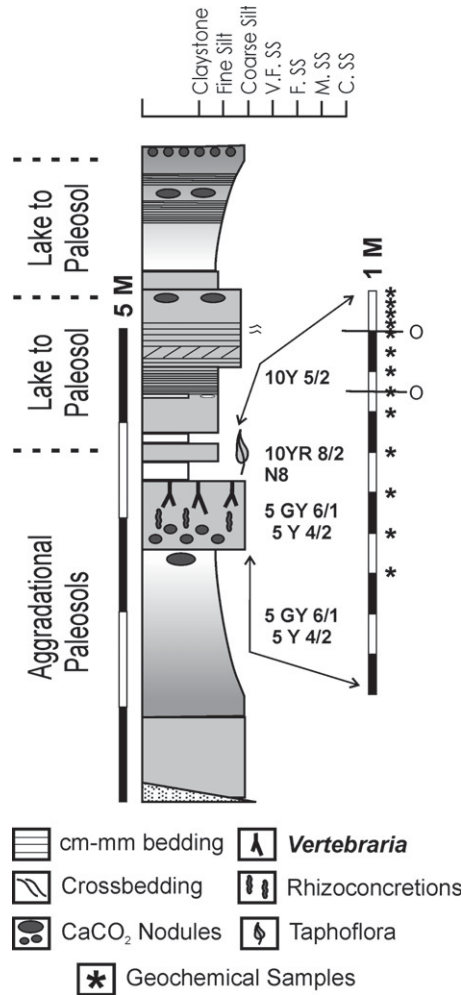


**Figure 3.** Stratigraphic section of the R61 outcrop exposure (31°55.927'S, 24°52.872'E, WGS84 Meridian) in which aggradational rooted paleosols underlie latest Changhsingian autochthonous forest-floor litters. Expanded section identifies the O-horizons are identified (O) and the stratigraphic position of samples analyzed geochemically. Carbonate nodules from which stable isotope values indicative of a transition from saturated sediment to well-drained conditions also are shown. Genetic interpretations of landscape evolution are from Prevec et al. (2010). SS—sandstone.

Wapadsberg Pass site exhibit greater weathering; only data from the R61 Highway site are presented.

Thin sections of paleosol-profile samples were made by Applied Petrographics and examined using a Leica DFC 290 Macroscope, equipped with a Leica Z6 apochromatic (APO) lens and image analysis software, and an Olympus BX41 petrographic microscope. Digital

images were acquired and examined to characterize the sedimentary and pedogenic fabrics, including microstratigraphic structures and other diagenetic features.

Paleosol-profile samples, beginning at a depth of 10 cm and continuing to a depth of 60 cm, were chosen for clay mineral analysis using X-ray diffraction (XRD). Rock chips without modern iron staining ( $N = 6$ ) were powdered in a ceramic mortar and pestle, sieved to separate the clay fraction, and the residuum adhered to glass slides using a filter-membrane peel technique (Pollastro, 1982). Four slides were prepared separately for analysis: One slide was left untreated; one slide was glycolated for 24 h to expand any expansible clay minerals that may have been present; and two slides were heated in a muffle furnace (one at 350 °C for 1 h to dehydrate the sample, the other at 550 °C for 1 h) to collapse the clay structures. Slides were analyzed using a Rigaku D-Max B two-axis X-ray diffractometer, and mineralogical identifications were made using Jade MDI 7 software at Colby College.

Powdered samples were analyzed for total organic carbon (TOC) and total organic nitrogen (TON) using a Perkin-Elmer 2400 CHNO/S Elemental Analyzer at Colby College. Samples were taken every 2 cm in the upper 10 cm, and every 5 cm in the remainder of the paleosol profile ( $N = 14$ ). Powders were analyzed in triplicate and averaged, and acetanilide standards ( $C = 71.09\%$ ,  $H = 6.71\%$ ,  $N = 10.36\%$ ,  $O = 11.84\%$ ) were run every 10 samples, as unknowns, to ensure data integrity and reproducibility. Replicate samples for C and N were within 0.2% and 1.8% relative standard error.

Paleosol-profile samples ( $N = 14$ ) were analyzed using X-ray fluorescence (XRF) at the Department of Geology, University of Maine–Farmington, to obtain major elemental data. After pretreatment in a muffle furnace for 1 h at 350 °C to drive off sorbed water, samples were milled to powder by hand using an agate mortar and pestle, each of which were cleaned with acetone to prevent cross-sample contamination. Powders were fused in glass disks (0.5 g of dried sample and 5.5 g of lithium metaborate + tetraborate flux in a platinum crucible) using an automated Phoenix fusion machine, which employs a preset menu for premelting, melting (1030 °C), and swirling to homogenize each sample. Once homogenized, the melt was poured into preheated platinum molds to cool.

Glass discs were analyzed for 10 major and eight trace elements using a Bruker S4 Pioneer XRF spectrometer, which uses standard wavelength dispersive (WD) XRF methodology with SpectraPlus software to collect and process data. Calibration lines were constructed using U.S.

Geological Survey (USGS) reference materials—G2, GSP-2, AGV-2, W2a, and BIR-1. Internal laboratory standards NJQ-2 and SBG-12 were used to monitor accuracy and precision. Precision values for the major and minor elements are 0.4% for  $SiO_2$ ; 0.1% for  $Al_2O_3$ ,  $K_2O$ , and  $Na_2O$ ; 0.01% for  $CaO$ ,  $Fe_2O_3$  (total), and  $MgO$ ; and 0.002% for  $MnO$ ,  $P_2O_5$ , and  $TiO_2$ . Trace-element precision values are: 10 ppm for Ba; 5 ppm for Cr, Sr, Zr, and Rb; and 2 ppm for Zn, Y, and Nb.

The XRF element-oxide data were used to calculate paleosol molecular weathering ratios, standard soil indices, and the chemical index of alteration (CIA). Soil molecular weathering ratios include base loss ( $[Ca, Mg, Na, K]/Ti$ ), clayeyness ( $Al/Si$ ), calcification ( $[Ca + Mg]/Al$ ), salinization ( $[K + Na]/Al$ ), mineralogical maturity ( $Si/Al$ ), and mineral assemblage stability ( $Fe/K$ ; Scheffler et al., 2003, 2006; Sheldon and Tabor, 2009). Element oxides were converted from wt% to molar abundance ( $wt\%/g$  element oxide/mol), and these values were used in spreadsheet calculations to create paleosol profiles. Standard soil indices (chemical index of alteration minus potassium [CIA–K]; Maynard, 1992) also were calculated using XRF element-oxide data to allow for comparison with modern soil types. Element-oxide abundances, based on XRF analysis for  $Al_2O_3$ ,  $CaO$ ,  $Na_2O$ , and  $K_2O$ , were converted from wt% to molar abundance, and the molar values were used to calculate CIA–K values with the equation (Sheldon and Tabor, 2009):

$$CIA-K = Al/(Al_2O_3 + CaO + Na_2O) \times 100. \quad (1)$$

Values were plotted versus paleosol depth to evaluate the amount of elemental loss or enrichment.

Fourteen powdered samples (25 mg) were treated with hydrofluoric acid digestion protocols for analysis in a Spectro Arcos inductively coupled plasma–optical emission spectrometer (ICP-OES) at Colby College to acquire trace-element and rare earth element (REE) data. Powders first were ashed in a muffle furnace at 550 °C for 3 h to remove organic matter and other volatiles (e.g.,  $SO_2$ ), followed by standard HF digestion procedure, with the additional step of heating samples in aqua-regia following HF treatment. Control blanks and USGS Icelandic Basalt BIR-1 standards (Gladney and Roelandts, 1988) also were digested using the same procedure and analyzed. Both major- and trace-element data were collected. Instrumental analytical uncertainty was 5%, with a detection limit of >10 ppb for most elements.

Fresh hand samples of calcite-cemented nodules ( $N = 15$ ) were collected from stratigraphic

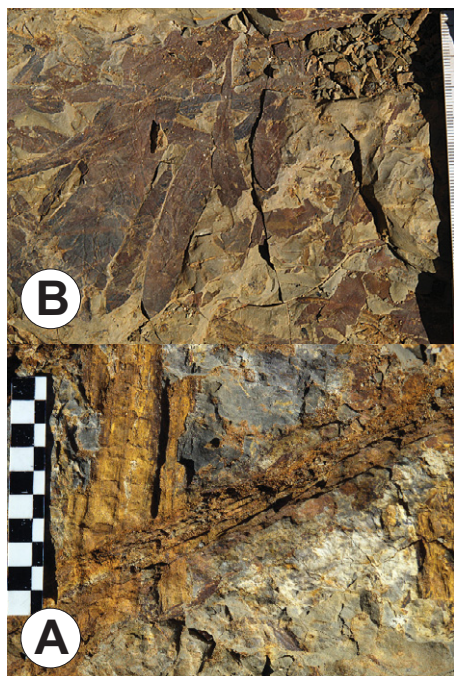


**Figure 4.** Macrofloral remains. (A) Two, wide-diameter, overlapping *Vertebraria* rooting structures that crosscut the bedding plane at a shallow angle. Woody roots are admixed with dispersed assemblage of degraded *Glossopteris* leaves and other unidentifiable aerial plant debris at ~25–30 cm depth in the profile. Scale in cm. (B) *Glossopteris* leaves in the upper forest-floor litter preserved as impressions. See Prevec et al. (2010) for plant taphonomy, systematics, and biostratigraphy. Scale in cm and mm.

horizons in both the New Wapadsberg Pass and Old Wapadsberg Pass sections (see supplemental data [see footnote 1]), extending down to 90 m below the end-Permian paleosol of DeKock and Kirschvink (2004), which is equivalent to the biostratigraphically defined Permian-Triassic boundary of Ward et al. (2000, 2005). Samples were thin sectioned to 70  $\mu\text{m}$  thickness, examined, and described petrographically. Micrite and microspar cement samples were drilled from thin sections or matching billets using an x, y, z drill mount. Sample powders were reacted with 100% orthophosphoric acid at 25 °C to produce  $\text{CO}_2$  (McCrea, 1950) and cryogenically purified. The stable carbon and oxygen isotope compositions of the extracted  $\text{CO}_2$  samples were measured at Southern Methodist University (SMU) using a Finnigan MAT 252 isotope-ratio mass spectrometer. For three samples, a large quantity of powder (200–400 mg) was gathered from each sample and treated with

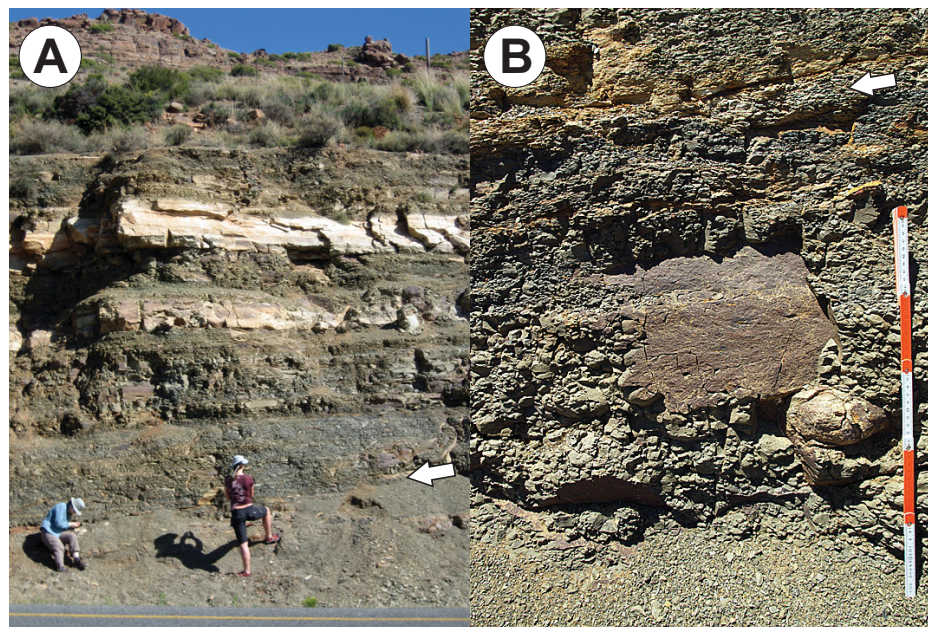


**Figure 5.** Images of the R61 exposure in outcrop. (A) Stratigraphic interval in which paleosols, fossil-plant assemblages, and overlying sediments occur. The arrow marks the position of the upper, well-preserved forest-floor litter. (B) Section in which two, aggradational paleosols occur, where the arrow marks the position of the upper, well-preserved litter horizon. Small, <10-cm-diameter, calcite-cemented, elliptical concretion can be seen adjacent to the scale. Scale in decimeters and centimeters.

concentrated HCl (12.1 N) to remove carbonate and eliminate it as a possible undesirable source of carbon during pyrolysis of organic matter. These were rinsed with successive aliquots of deionized  $\text{H}_2\text{O}$  until the rinse water remained at the original pH (~5.6) after at least 10 min of contact with the acid-leached sample. These organic-enriched residues were freeze-dried to remove sorbed water, and the carbon content and  $\delta^{13}\text{C}$  values were determined from  $\text{CO}_2$  produced by closed-system combustion of the organic matter following the methods of Boutton (1991).

Measured isotope values are reported in permil notation:

$$\delta^{13}\text{C} \text{ (or } ^{18}\text{O)} = (R_{\text{sample}}/R_{\text{standard}} - 1) \times 1000, \quad (2)$$

where  $R = ^{13}\text{C}/^{12}\text{C}$  and  $^{18}\text{O}/^{16}\text{O}$  for carbon and oxygen, respectively. The international reference material used to report isotope values of calcite is Peedee belemnite (PDB; Craig, 1957). Routine analyses ( $N = 9$ ) of  $\text{CO}_2$  extracted from an in-house standard of Carrera marble yielded  $-2.33\text{‰} \pm 0.05\text{‰}$  and  $-5.91\text{‰} \pm 0.11\text{‰}$  for carbon and oxygen isotope compositions, respectively. Routine analyses ( $N = 8$ ) of  $\text{CO}_2$  combusted from an in-house standard of graphite yielded  $-25.98\text{‰} \pm 0.07\text{‰}$  for carbon isotope composition.

## RESULTS

The stacked paleosol sequence at Wapadsberg Pass is characterized by four lithofacies; in descending stratigraphic order, they are a claystone, siltstone, coarse siltstone, and sandy siltstone (Fig. 3). The paleosurface (10 cm depth) is immediately below a white to pale yellowish orange (10YR 8/6), tuffaceous claystone in which impressions of small *Glossopteris* leaves are preserved (0 cm; Figs. 4 and 5B). The base of the stacked sequence is marked by the lowest extent of in situ rooting structures and the sporadic occurrence of small (<10 cm), carbonate-cemented nodules (Fig. 4B) in sandy siltstone. The thickness of the interval is ~70 cm along the R61 road cut, but it varies laterally in the donga sections at Old Wapadsberg Pass to a minimum of 40 cm due to available exposure. Lithologies appear massive and weathered in outcrop and color ranges from olive-green (5Y 4/1) to grayish olive (10Y 4/2) or greenish-gray (5GY 6/1). Structures include: (1) a 2-cm-thick, root-penetrated white claystone (tuffite) at 20 cm depth; (2) rounded white claystone (tuffite) spherical clasts,  $\geq 3$  cm in diameter, concentrated at ~30 cm depth and found to a depth of 50 cm; and (3) modern iron staining concentrated along a few bedding horizons. There is little evidence of any primary sedimentary structures in outcrop,

but millimeter- to centimeter-scale planar beds and occasional ripples occur in the siltstone that overlies the paleosol O-horizon (Prevec et al., 2010; Fig. 3).

Siltstone, with coarse siltstone to very fine sandstone grains, occurs directly beneath the tuffite and contains a thin bed of entire, partial, and degraded *Glossopteris* leaves considered to be the former soil-air interface (Fig. 6A). Scattered vertical and inclined *Vertebraria* roots are present and account, in part, for the absence of any primary structure in parts of the profile. Bioturbation structures are evident in the upper few centimeters, beneath which opaque, black dispersed organic debris and weak, millimeter-scale bedding are preserved to a depth of 20 cm (Fig. 6B). A strong discoloration due to iron staining coincides with the relative enrichment of organic matter (OM) at 8 cm depth, and bedded *Glossopteris* leaves at this horizon are accentuated by a thin coating of white claystone. In thin section, roots occur as vertically to subvertically oriented, millimeter-scale, amber-colored features. Sandy siltstone with sub-angular to rounded clasts, ~1 mm in diameter, occurs beneath a depth of 20 cm and appears bioturbated (Figs. 6C and 6D). The remaining section is a massive and homogeneous siltstone, with small-scale, primary structures evident at a depth of ~70 cm. A massive, fining-upward sequence of siltstone occurs below 70 cm depth and contains dispersed calcareous nodules (5–10 cm in diameter) and spherical clay balls (0.3–2 cm in diameter).

### Organic Carbon and Nitrogen Trends

All TOC values are <1%, with a minimum value of 0.14 ( $\pm 0.010$ ) at a depth of 4 cm and a maximum value of 0.42 ( $\pm 0.003$ ) at a depth of 8 cm (Fig. 7A). Two positive trends in TOC values are observed. Total nitrogen trends parallel those of TOC with values an order of magnitude smaller, ranging from a minimum of 0.02 ( $\pm 0.002$ ; 50 cm depth) to a maximum of 0.48 ( $\pm 0.016$ ; 30 cm depth). TOC:TON values are <10, and average 6.3.

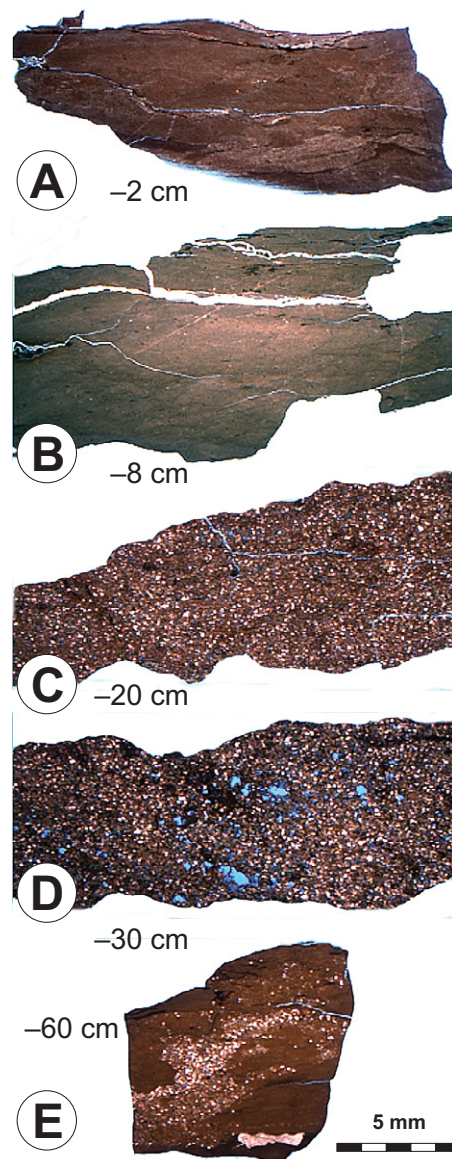
### Geochemical Trends

The profile pattern in TOC also is reflected in plots of the soil molecular weathering ratios versus profile depth (Fig. 7) and chemical index of alteration minus potassium (CIA–K) trends (Fig. 8). Excursions in the profile of various proxies demonstrate their sequenced nature.

### Soil Molecular Weathering Ratios

Each calculated soil molecular weathering ratio acts as a proxy for different pedogenic

**Figure 6. Selected thin sections of Wapad-berg Pass siltstone interval. (A) Thin section at a profile depth of –2 cm in which bedded forest litter can be seen in the upper part, and evidence of bioturbation occurs near the bottom of the slide. (B) Thin section at a profile depth of –8 cm in which black, opaque organics in the upper part and bioturbation near the base are visible. A few quartz clasts can be seen in the siltstone. (C) Thin section at a profile depth of –20 cm, where the sediment becomes a sandy siltstone and iron staining appears around vertical, millimeter-scale rooting structures. (D) Thin section at a profile depth of –30 cm, where organics are seen in the upper-right corner of the slide. (E) Thin section at a profile depth of –60 cm where faint, relict bedding; evidence for soft-sediment deformation or bioturbation; and a flattened, deformed tuffite clast are seen. All slides at same magnification; scale equals 5 mm.**



properties or processes. These include base loss (Fig. 7B), clayeyness (Fig. 7C), mineral assemblage stability (Fig. 7D), calcification (Fig. 7E), salinization (Fig. 7F), mineral maturity (Fig. 7G), and weathering intensity (Fig. 7H; Sheldon and Tabor, 2009). These values (see: supplemental data Table DR2 [see footnote 1]) plotted versus profile depth exhibit similar sharp excursions and trends and fall into two groups, with the exception of base loss. The first includes clayeyness and mineral assemblage stability, and the second includes calcification, salinization, and mineralogical maturity. Inverse trends characterize these two groups with either a prominent positive or negative excursion at 25 cm depth, with similar values and trends recorded for the intervals between 10 cm to 25 cm, and 30 cm to 60 cm depth.

Base loss is a proxy for the degree to which a soil is leached, wherein Ca, Mg, Na, and K are translocated relative to Ti, which accumulates within the soil profile (Sheldon and Tabor, 2009). The Mg/Ti and K/Ti profiles show little variation with depth, except for a single, sharp decrease in Mg loss at the 8–10 cm depth interval above the contact with the former O-horizon (Fig. 7B). In the cases of Na/Ti and Ca/Ti, both ratios exhibit a trend of increasing base loss with paleosol depth. Values approaching 1 occur at: (1) 10 cm, at the contact of the plant-fossil interval and overlying tuffite and siltstone; (2) at 25 cm depth, corresponding to the second fossilized litter horizon; and (3) at 60 cm.

Clayeyness, defined as the Al/Si ratio (Sheldon and Tabor, 2009), is a proxy for hydrolysis and clay-mineral formation as Al accumulates

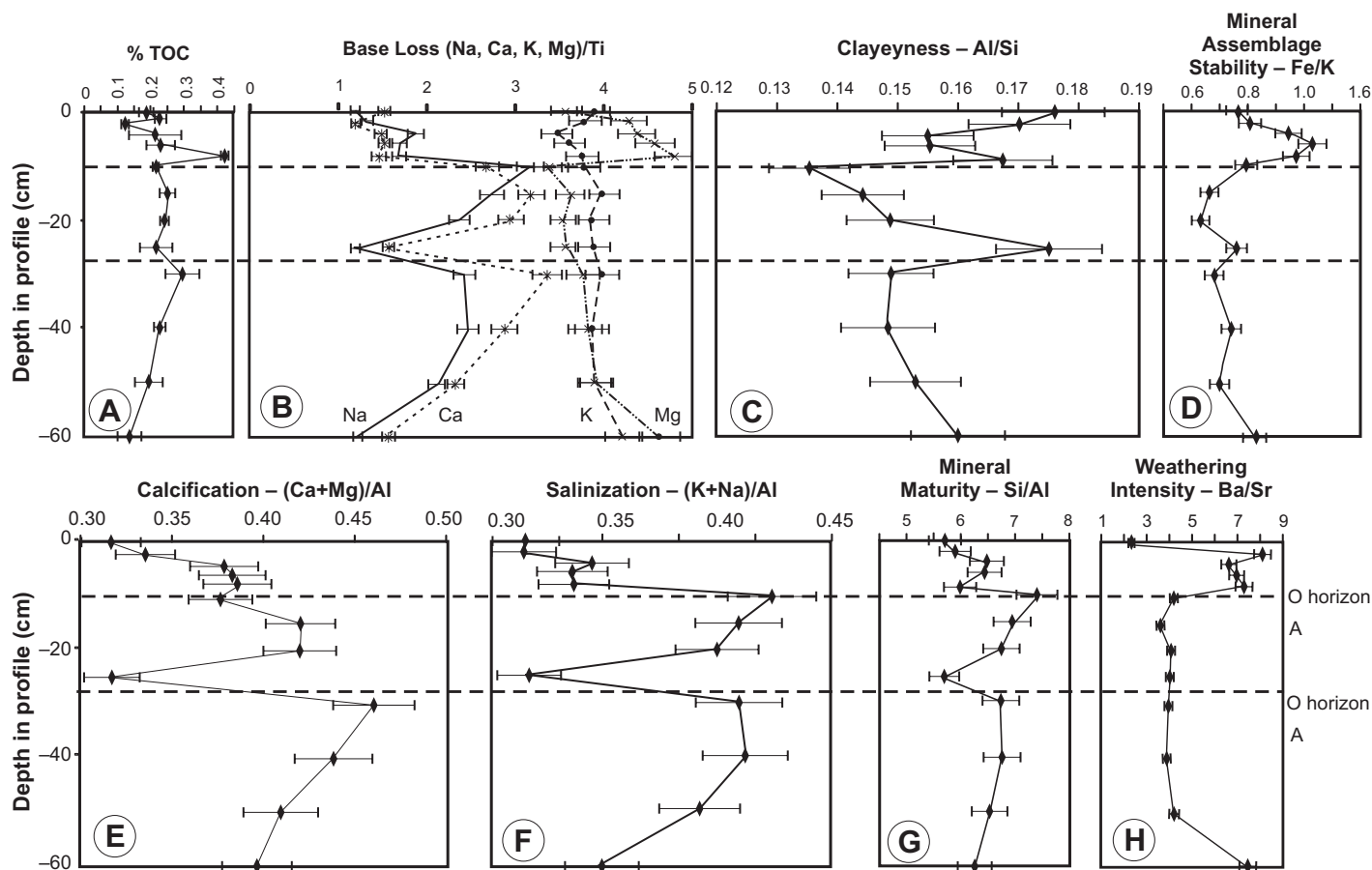


**Figure 7.** Geochemical proxy profiles of Wapadsberg Pass aggradational paleosols (see text for details). The top of each mineral soil is a wide dashed line across the plots, and the O- and A-master horizons are marked. (A) Total organic carbon showing positive excursion at  $-10$  cm and at  $-25$  cm depths, marking the former soil-air interfaces of the landscape. The well-preserved fossil-plant litter is in the upper 10 cm of the interval. (B) Base loss profiles for Na/Ti (solid black line), Ca/Ti (short dash line), K/Ti (long dash line), and Mg/Ti (dash and dotted line). Error bars at 5% are provided for each sample. (C) Clayeyiness (Al/Si). (D) Mineral assemblage stability (Fe/K). (E) Calcification ( $[Ca + Mg]/Al$ ). (F) Salinization ( $[K + Na]/Al$ ). (G) Mineral maturity (Si/Al). (H) Weathering intensity (Ba/Sr). Data provided in supplemental data Tables DR2 and DR4 (see text footnote 1)

in clays relative to the siliceous parent material. Maxima at 10 cm and 25 cm depth correspond to the stratigraphic position of bedded plant debris (Fig. 7C) and support the stacked paleosol interpretation, which also is mimicked, to a lesser extent, in the mineral assemblage stability plot (Fig. 7D). XRD analyses of the clay fraction from samples at 10 cm and 60 cm depth indicate the presence of illite (which may be diagenetic alteration of montmorillonite), quartz, albite, and clinocllore.

Calcification ( $[Ca + Mg]/Al$ ; Fig. 7E) and salinization ( $[K + Na]/Al$ ; Fig. 7F) trends, proxies for the abundance of carbonates and salts in a soil profile (Sheldon and Tabor, 2009), and mineral maturity (Si/Al; Fig. 7G) are similar. Maximum negative excursions occur above 10 and 25 cm depths, corresponding to the surfaces on which plant debris accumulated and is preserved.

CIA-K values (see supplemental data Table DR3 [see footnote 1]) and trends (Fig. 8) range

from a low of 73, at 30 cm depth, to maxima of 85–87 at three horizons ( $-60$  cm,  $-25$  cm,  $-2$  cm). Maxima are found at preserved litters, and similar, decreasing CIA-K value trends below these maxima appear to delimit each soil thickness.

#### Trace Elements

Trace-element abundances are presented in the supplemental data (see supplemental data Tables DR4 and DR5 [see footnote 1]). Concentrations of Ba, Cr, Cu, Ni, and Zn are comparatively high in the stacked paleosols when compared with the whole-rock data presented by Coney et al. (2007).

The Ba/Sr ratio is a proxy for trace-element leaching in response to weathering intensity (Sheldon and Tabor, 2009). No discernible trend in the Ba/Sr ratio occurs (Fig. 7H), with maxima found in the overlying white claystone (tuffite) lithology (Prevec et al., 2010).

#### Stable Isotope Trends

Stable isotope values from micritic and microspar ( $<20 \mu m$ ) calcite cements assessed in carbonate-cemented nodules over the 90 m of stratigraphic section sampled (see supplemental data Fig. DR1 [see footnote 1]) exhibit two different stratigraphic trends (Table 1). Although some variability exists in the  $\delta^{18}O$  values, with PDB values ranging from  $-14.7\text{‰}$  to  $-21.8\text{‰}$ , no clear trend is identifiable up section (Table 1). In contrast, calcite  $\delta^{13}C_{PDB}$  values range from a high of  $-5.3\text{‰}$ , immediately above Prevec et al.'s (2010) thinly laminated siltstone facies overlying the autochthonous flora, to low values of  $-16.9\text{‰}$  within 6 m of the vertebrate-defined Permian-Triassic boundary. Plots of calcite  $\delta^{13}C$  values versus the stratigraphic position of parent nodule show a clear trend (Fig. 9). Relatively negative  $\delta^{13}C$  values at the base of the section trend toward more positive values up to 60 m

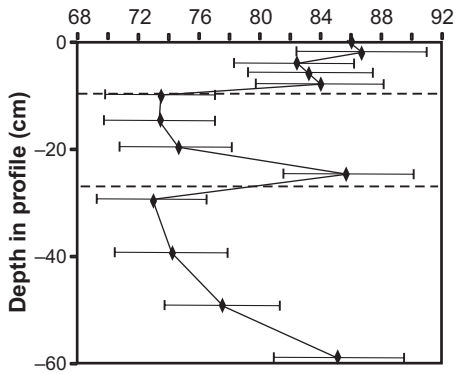


**Figure 8.** Plot of siltstone profile of CIA-K (chemical index of alteration minus potassium) along with 5% error bars. Positive excursions at -10 cm and at -25 cm depths mark the former soil-air interfaces of the landscape. High CIA-K indices signal soil development under warm, wet climatic conditions for the entire 60 cm siltstone profile.

below the Permian-Triassic boundary and thereafter trend toward more negative values up to the vertebrate-defined Permian-Triassic boundary (Ward et al., 2000).

## DISCUSSION

The Wapadsberg Pass section plays a key role in our understanding of temporal trends in landscape development and climate prior to the biostratigraphically defined Permian-Triassic event in the Southern Hemisphere (Rubidge,

1995; Ward et al., 2005). The current hypothesis links biodiversity extinction and turnover to changes in Karoo Basin fluvial architecture in response to climate change in the transition from the Balfour to Katberg Formations (Smith, 1995; Ward et al., 2000; Smith and Ward, 2001). This changeover is interpreted as the sedimentological response to increasing aridity (Smith, 1995; Smith and Ward, 2001), although an increasingly wet and seasonal trend for the same interval also has been reported (Retallack et al., 2003). The currently accepted model implicates increasing aridity as the factor that drove the *Glossopteris* flora, a wetland biome (Greb et al., 2006), to extinction coincident with the end-Permian crisis (Smith and Ward, 2001). Consequently, the loss of primary producers resulted in ecosystem collapse hypothesized as being coeval with the marine boundary event (Ward et al., 2000, 2005; Shen et al., 2011). If latest Permian climate change (Scheffler et al., 2006) was a response to increasing global atmospheric gas concentrations and warming, evidence of an aridification trend should occur in preboundary sedimentary sequences.

Paleontological, sedimentological, and geochemical data support the presence of two stacked wetland Protosols 70 m below the Permian-Triassic boundary at Wapadsberg Pass. Autochthonous, forest-floor litters (Fig. 5B; Prevec et al., 2010) preserved above woody *Vertebraria* (Fig. 4A) and millimeter-scale nonwoody rooted sediment are clear evidence of former buried landscapes (DiMichele and Gastaldo, 2008). The presence of primary sedi-

mentary structures and unbioturbated tuffite in the soil profiles reflects immature pedogenesis, and the weakly developed nature of these paleosols is supported by the geochemical data (Fig. 7). Hence, these Protosols developed under a high regional water table that, in turn, required sufficient annual rainfall to maintain these physical conditions. Wetland conditions are not restricted to these Protosols, as trends in paleosol carbonate  $\delta^{13}\text{C}$  values indicate calcite precipitation primarily under continued wet, saturated soil conditions through most of the latest Changhsingian (see following discussion; Tabor et al., 2007).

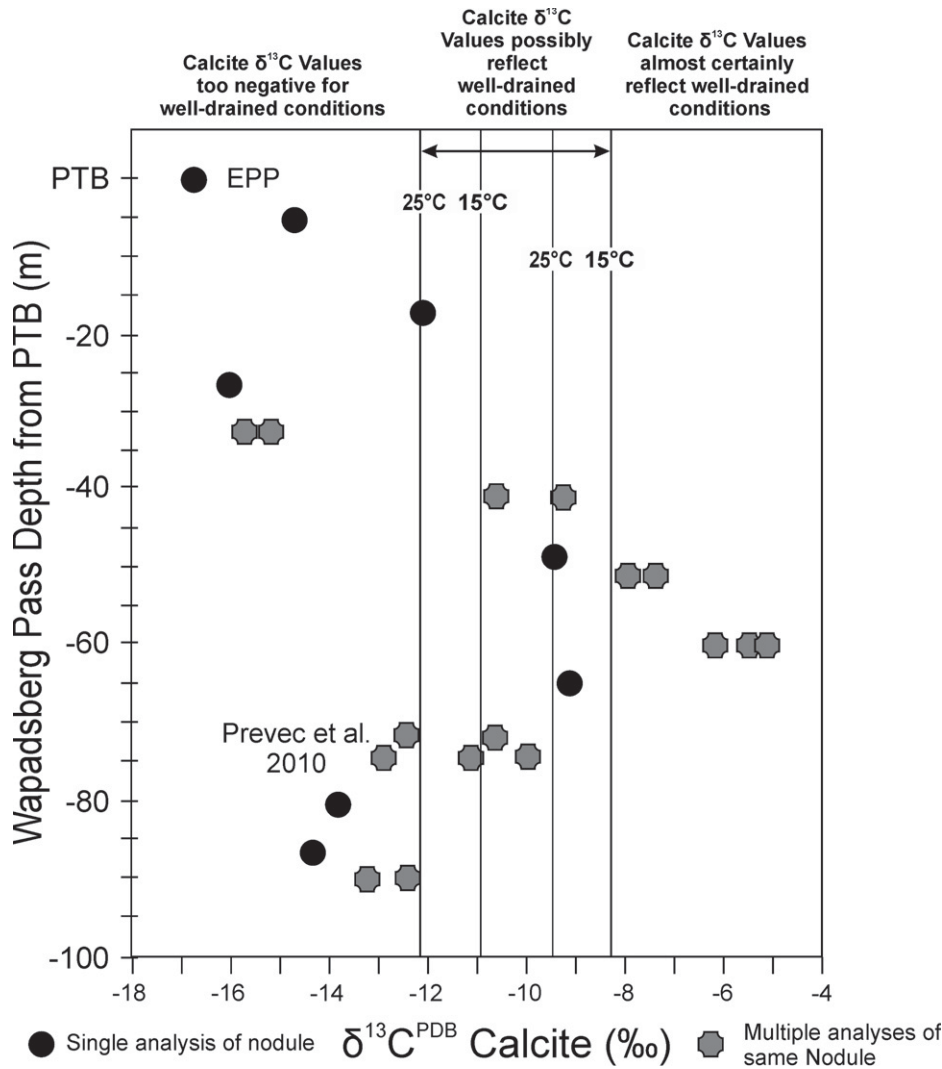
Of some interest are the low TOC:TON Protosol ratios (<10), which may be indicative of a high proportion of algal versus terrestrial OM inherited contribution. First used in marine environments to differentiate the source of OM contribution to a sedimentary system (e.g., Meyers, 1994), but equally applicable to freshwater and terrestrial regimes (e.g., Aitkinhead and McDowell, 2000), C/N ratios are based on Redfield stoichiometry—the atomic ratio of carbon, nitrogen, and phosphorus in phytoplankton. Algal debris exhibits C/N ratios ranging between 4 and 10, whereas vascular land plants exhibit C/N ratios >20 because of a different cell wall chemistry. Hence, it is possible that terrestrial-derived organics had not yet accumulated in significant quantities in either Protosol, reflecting substrate immaturity, either due to retention of an algal signature in overbank deposits or of a soil algal component (Vyzamal, 1995). Alternatively, the low values may have

TABLE 1. STABLE OXYGEN ( $\delta^{18}\text{O}$ ) AND CARBON ( $\delta^{13}\text{C}$ ) ISOTOPIC VALUES\*

Wapadsberg Pass sample number	Stratigraphic depth from PTB (m)	Petrographic texture	$\delta^{18}\text{O}_{\text{PDB}}$ (‰)	$\delta^{18}\text{O}_{\text{SMOW}}$ (‰)	$\delta^{13}\text{C}_{\text{cc}}$ (‰)
23606_16	0	Micrite; microspar	-21.5	8.7	-14.9
23606_15	-6	Micrite; microspar	-21.3	9	-16.9
23606_18	-18	Micrite; microspar	-21.2	9	-12.2
23606_19	-27	Micrite	-21.2	9	-16.1
23606_21	-33	Micrite inclusion	-21	9.3	-15.8
23606_21	-33	Micrite inclusion	-21.8	8.4	-15.3
23606_9a	-41	Micrite	-21.5	8.7	-10.7
23606_9b	-41	Microspar	-21.6	8.6	-9.3
23606_22	-49	Micrite	-21.7	8.5	-9.5
23606_8	-51	Gray microspar	-15.4	15	-7.5
23606_8	-51	Red microspar	-14.7	15.8	-8
23606_23	-60	Gray rind	-21.3	9	-5.5
23606_23	-60	Gray with dendritic opaques	-21.1	9.2	-6.2
23606_23	-60	Framboids	-21	9.3	-5.3
21606_13	-65	Micrite	-21.5	9.8	-9.17
21606_12	-72	Micrite; microspar	-17.2	13.2	-10.7
21606_12	-72	Micrite; microspar	-21.7	8.5	-12.5
23606_24	-75	Micrite associated with gypsum	-21.6	8.6	-10
23606_24	-75	Micrite associated with organics	-21.8	8.4	-13
23606_24	-75	Micrite associated with pyrite	-21.5	8.7	-11.2
21606_11	-80.5	Micrite	-21.9	8.3	-13.9
21606_10	-86.5	Micrite	-16.4	14	-14.4
21606_9	-90	Micrite	-21.7	8.5	-12.5
21606_9	-90	Micrite; microspar	-21.9	8.3	-13.3

Note:  $\delta^{18}\text{O}$  values are reported relative to Peedee belemnite (PDB) and standard mean ocean water (SMOW);  $\delta^{13}\text{C}$  values are reported relative to PDB. See supplemental data (text footnote 1) for stratigraphy and sampling horizons; cc—calcite.

\*Obtained from micrite or microspar cements from calcite-cemented nodular horizons exposed at Wapadsberg Pass to a depth of 90 m below the vertebrate biostratigraphically defined Permian-Triassic boundary (PTB).



**Figure 9.** Plot of stratigraphic position of calcareous nodules relative to the Permian-Triassic boundary (PTB; at 0 m) as defined by vertebrate biostratigraphy at the Wapadsberg Pass section versus calcite  $\delta^{13}\text{C}$  values of those nodules with micrite or microspar cements. Black circles represent paleosol profiles from which only one paleosol nodule  $\delta^{13}\text{C}$  value was determined, whereas gray plaques represent paleosol profiles where multiple (i.e.,  $n = 2$  or  $3$ ) paleosol nodule  $\delta^{13}\text{C}$  values were determined. Fields in which  $\delta^{13}\text{C}$  values reflect crystallization under well-drained or wetland conditions are plotted, indicating that most carbonate nodules precipitated under closed, wet sediment conditions (Tabor et al., 2007). EPP—End Permian Paleosol of DeKock and Kirschvink (2004).

been influenced by nitrogen loss in response to OM decomposition.

Geochemical proxies parallel TOC trends with both positive or negative excursions marking the tops of Protosols (Figs. 7 and 8). Base loss measures the amount of Ca, Mg, Na, and K leached relative to Ti, wherein both Ca and Na preferentially are mobilized in soils that experience a high water table; these elements are more water soluble than Mg and K (Sheldon and Tabor, 2009). A decrease in Ca and Na values down paleosol profiles, relative to

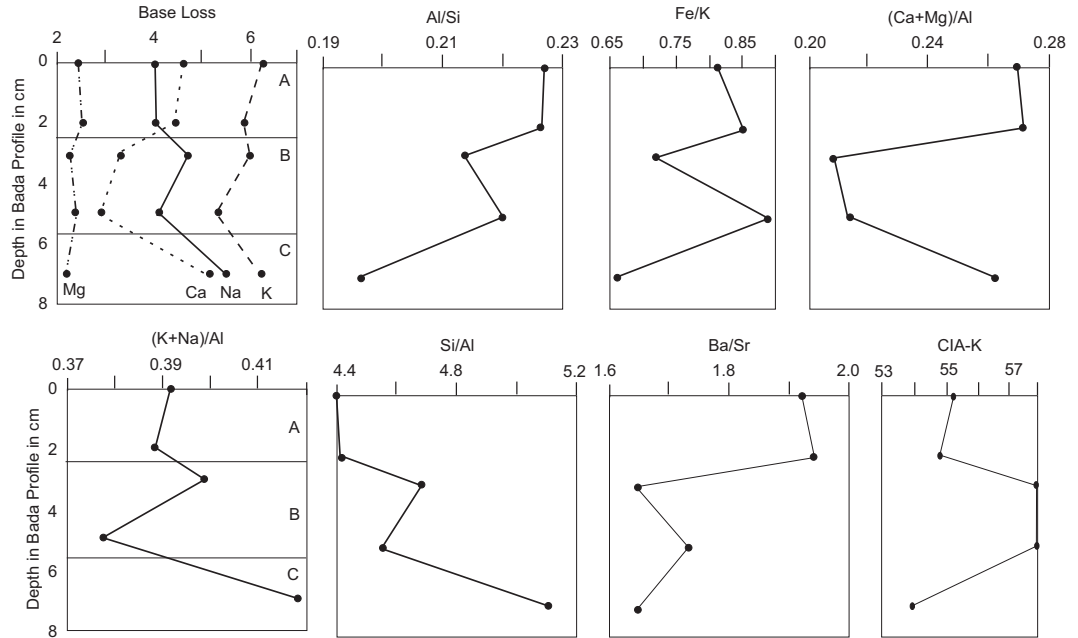
consistent Mg and K profile trends, and those for clayeyness, calcification, salinization, and mineral assemblage maturity define the two Protosols. Although such trends also may be a function of diagenetic alteration, the short stratigraphic distance over which these occur is more likely an original signature. Barium: strontium values are an indication of weathering intensity, and paleosol profiles exhibiting higher Ba/Sr ratios in the B horizon reflect greater leaching (Sheldon and Tabor, 2009). This situation is not found at Wapadsberg Pass (Fig. 7H), pointing to

the absence of any B horizon development and indicative of paleosol immaturity.

B horizons are reported from Late Permian paleosols, but it is difficult to compare Wapadsberg Pass geochemical proxy trends to those presented by Retallack et al. (2003). This is because: (1) chemical data exist for only one paleosol type (Bada); (2) the locality from which this paleosol was collected and analyzed is cryptic (Retallack et al., 2003, GSA Data Repository item 2003122); and (3) the data are plotted at very coarse resolution. The Bada soil is: characterized as a thin, fine-to-medium sandstone, sandy siltstone, or siltstone paleosol; figured at 7 cm thickness (but reported to be as thick as 54 cm; GSA Data Repository item 2003122); and subdivided into A, Bk, By, and C horizons (Fig. 10). There is a notable difference between the Bada paleosol and Wapadsberg Pass Protosol profiles when the supplemental repository data from Retallack et al. (2003) are plotted at the same scale as in the current contribution.

The CIA provides information about weathering profiles as a function of climate. Because mobile alkali and alkaline earth elements form soluble cations during normal weathering processes and are translocated or removed, high CIA values reflect intense weathering conditions (Nesbitt and Young, 1982) under warmer and wetter climate states. It is known that there exists a potential addition of elements to a lithology via metasomatism or illitization of clay minerals under submetamorphic burial conditions. Due to this possibility, Sheldon and Tabor (2009) noted that some authors remove K from the calculation. Dolerite intrusions in the Karoo Basin are ubiquitous, and illite is present in Wapadsberg Pass samples; hence, only CIA-K values are reported here. Maximum CIA-K values are  $>80$  near the base of each Protosol, and profile trends mimic those of other geochemical proxies (Fig. 8). The average Protosol CIA-K value is 77, but the lower values in the profile do not correlate with a more well-developed horizon; this feature probably reflects an inheritance prior to pedogenesis. In contrast, Retallack et al. (2003) reported an average CIA-K value of 56 for the Bada paleosol (a gleyed Calcisol; GSA Data Repository item 2003122), which is lower than a recalculated value of 64 and those in the current study (see supplemental data Table DR3 [see footnote 1]). The high CIA-K values, coupled with soil colonization by *Glossopteris*, indicate that these pre-extinction landscapes were not subjected to seasonal dry conditions but were maintained under a high water table. It is not possible to extrapolate calculated proxy values to estimate paleoclimate conditions at the time of Protosol genesis because there is no recognizable B horizon (e.g., Maynard, 1992;

**Figure 10.** Geochemical proxy data from the 7-cm-thick Bada paleosol profile of Retallack et al. (2003) exposed at Lootsberg Pass (Fig. 1), reported to be ~20 m below the Permian-Triassic boundary as defined by the “event bed” or “laminite interval” (see Gastaldo et al., 2009; Gastaldo and Neveling, 2012). Data and soil horization from GSA Data Repository item 2003122 are plotted at a comparable scale as those for the Wapadsberg Pass aggradational paleosols; base loss relationships are the same as in Figure 7. Chemical index of alteration minus potassium (CIA-K) values for the Bada paleosol type are reported to range between 54 and 58, but see supplemental data Table DR3 (see text footnote 1), where an average value of 64 is calculated from the same data.



Sheldon et al., 2002; Sheldon and Tabor, 2009). However, Wapadsberg Pass values can be used to better constrain previously interpreted basinal trends using the CIA proxy.

In a broad study of the Karoo Basin, focused on the Dwyka and Ecca Groups (Fig. 2), Scheffler et al. (2003, 2006) concluded that geochemical proxy signatures indicate an overall, unidirectional climate change from the late Pennsylvanian to the Triassic. They documented strong oscillations between cold-and-dry to humid-and-warm conditions in the Dwyka Group, reflecting the waxing and waning of late Pennsylvanian (Gzhelian) and Early Permian (Artinskian; Stollhofen et al., 2008) continental glaciation. Dwyka Group CIA-K values range between 50 and 60, followed by a steady increase into the Middle Permian Ecca Group, where a maximum value near 90 is reported in the Prince Albert Formation (Scheffler et al., 2006; Fig. 2). This value—indicative of the highest temperatures, the wettest environments, and the spread of the *Glossopteris* biome—is associated with peat accumulation following deglaciation. Subsequently, the overall Middle Permian CIA trend hovers around 65, decreasing to 50 in the Whitehill and Collingham Formations (Fig. 2). These low values are interpreted to indicate the onset of an arid climate, although the change also is noted to be associated with a higher proportion of feldspar in the coarser-grained Collingham Formation sediments (Scheffler et al., 2006). Very coarse stratigraphic sampling from the Middle to Upper Permian and Triassic,

based on Kalahari Basin drill core, exhibits an overall decreasing CIA trend, with a maximum of 70 near the base of the Beaufort Group and a minimum near 55 in the Lebung Group of Late Triassic age (Bordy et al., 2010). Scheffler et al. (2006) noted a correlation between changes in geochemical proxies and the first appearance of red beds (but see Sheldon [2005], who argues that red coloration in Permian paleosols may not be a primary character), and the decreasing CIA trend is interpreted as a change from warm, humid to warm, arid conditions.

The Wapadsberg Pass CIA-K values are indicative of warm, humid and, most probably, seasonally wet conditions prevailing across the landscape prior to the vertebrate-defined Permian-Triassic boundary. These are consistent with values reported by Scheffler et al. (2003, 2006) for the Early to Middle Permian, also interpreted to reflect high weathering rates under moist climatic conditions. Climate is modulated by a number of intrinsic and extrinsic factors, and cyclical variation across the wet-to-dry spectrum is expected to be reflected in the sedimentological character of continental stratigraphic sequences (Gastaldo and Demko, 2010). There is but one concretionary interval in the 90 m of Wapadsberg Pass stratigraphy leading up to the vertebrate-defined Permian-Triassic boundary that exhibits stable isotope geochemical evidence for carbonate cements having been precipitated in equilibrium with atmospheric conditions under a more seasonally dry and evaporative climate (Fig. 9; Reid et al.,

2007; see following discussion). These data originate from two paleosols (see supplemental data [see footnote 1]) where small, round, regularly spaced nodules formed around vertical roots in positions of former mud cracks (Prevec et al., 2010; Fig. 4).

Few elemental data sets exist for the stratigraphy approaching the vertebrate-defined Permian-Triassic boundary in the Karoo Basin, and published data are only reported for sections at Commandodrift Dam and Wapadsberg Pass (Coney, 2005; Coney et al., 2007). Coney et al. (2007) identified the Permian-Triassic boundary as the contact between the Elandsberg and Palingkloof Members of the Balfour Formation (Fig. 2), where there is a reported change in siltstone color from dark-gray and green-gray to red-brown. They sampled ~7 m of the uppermost Elandsberg Member (Fig. 2) and 2.1 m of the lowermost Palingkloof Member (Fig. 2) at the Old Wapadsberg Pass section, although their global positioning system (GPS) coordinates plot west of the locality identified by Ward et al. (2000) and from which new fossil-plant assemblages are reported (Gastaldo et al., 2005; Prevec et al., 2010; Fig. 1). As noted by others, intervals of alternating sandstone and siltstone leading up to the vertebrate-defined boundary are capped by concretion-bearing green siltstone; intervals above the boundary are described as red-brown mudstone with overlying channel-form sandstone and siltstone. Hence, Coney et al.'s (2007) samples originate ~63 m above those of the current study.

No change in geochemical composition of either major- or trace-element concentrations is reported across the paleontologically defined Permian-Triassic boundary, except for an increase in  $\text{Fe}_2\text{O}_3$  (Coney et al., 2007). No interpretation has been placed on any depositional environment in the Permian-Triassic boundary interval at either Commando drift Dam or Wapadsberg Pass, and Coney et al. (2007) relied on the previously published reports of Ward et al. (2000), Smith and Ward (2001), and Retallack et al. (2003) for context. That context interprets mudstone intervals as overbank and floodplain deposits and paleosols in the Upper Permian Elandsberg and informal lower Palingkloof Members, and as floodplain deposits and paleosols in the informal upper Palingkloof Member assigned to the Triassic. If we accept this interpretation, that fine clastics immediately beneath and above the vertebrate-defined Permian-Triassic boundary represent paleosols (the EPP of De Kock and Kirschvink, 2004), then CIA-K values can be calculated for Coney et al.'s (2007) major-element data from Wapadsberg Pass and plotted against the stratigraphy reported herein (Fig. 11). The average CIA-K value for Elandsberg Member lithologies is 60, whereas that value is 70 for the Palingkloof Member (see supplemental data Table DR3 [see footnote 1]). These values lie between those reported herein for New Wapadsberg Pass Protosols and that of Retallack et al. (2003; GSA Data Repository item 2003122, their table 9).

Average elemental concentrations in New Wapadsberg Pass Protosols are similar to those reported by Coney et al. (2007) in both the Elandsberg and Palingkloof Members (see supplemental data Table DR4 [see footnote 1]). The few exceptions include: Co, Ni, Zn, Gd, and Nd, which are higher; and Sr, La, and Y, which are lower. Their data, together with the current results, indicate that there is little geochemical difference in either the uppermost ~70 m of the latest Changhsingian or the first few meters of what is considered to be the Induan (Coney et al., 2007). However, there are important differences in the concentrations of some trace elements when these Permian data are compared to modern soils.

### Implications of Paleosol Geochemistry

Assuming that paleosol matrix concentrations of trace elements are indicative of Permian soil-solution chemistries, chemical compositions of Wapadsberg Pass Protosols and those of Coney et al. (2007) are higher than values reported for many present vegetated soil profiles. Some difficulty exists in making any direct comparisons with Holocene baseline concentrations because

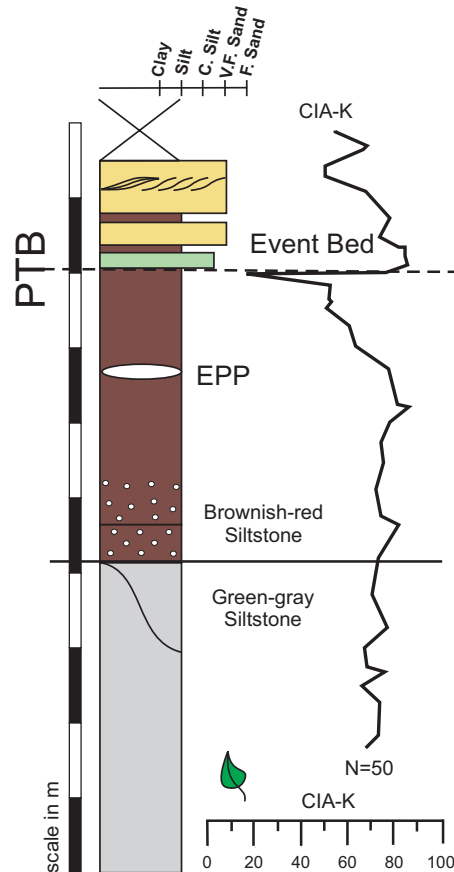


**Figure 11. Chemical index of alteration minus potassium (CIA-K) values calculated from data provided by Coney et al. (2007, Table 2) for the Permian-Triassic boundary (PTB) interval at (Old) Wapadsberg Pass, plotted against a high-resolution stratigraphy of the section (from Gastaldo et al., 2005; Reid et al., 2007). Retallack et al. (2003) reported the presence of Zam paleosols to a depth of -6 m at Lootsberg Pass (Fig. 1). EPP—End Permian Paleosol of DeKock and Kirschvink (2004).**

modern data are dependent on the dominant soil-forming factors, sample material, grain size, and extraction methodology. Modern soils (Entisols and Inceptisols) that are morphologically equivalent to Protosols have diverse mineral assemblages and typically show little evidence of weathering (Lynn et al., 2002). The low rate of weathering in Permian Protosols, as a function of either high soil moisture or high aggradation rates, or both, may be one factor to account for high elemental concentrations of base cations reported herein and by Coney et al. (2007). Similarly, because the mineralogy of the parental material for these paleosols dictates the amount of any trace element in the pedon (Burt et al., 2003), latest Permian elemental concen-

trations may be related to the composition of detrital sediments originating from the Cape Fold Belt and volcanoclastic sediments derived from regional volcanism, the latter evidenced by tuffite in both the paleosol profiles and elsewhere in the Wapadsberg stratigraphy (Prevec et al., 2010). Nevertheless, higher concentrations of one or more trace elements may account for the small size of latest Permian glossopterid leaves, as an alternative to the hypothesis that implicates leaf size as a reflection of a more seasonally arid, pre-event climate (Retallack et al., 2003).

Toxic elements to plant growth include Fe, Mn, Zn, Ni, Cu, Ba, and Cr, and inhibition happens when one or more of these occur in high soil concentrations; in contrast, Mn, Zn, and Cu may limit growth if soil concentrations are too low (e.g., Hunt, 1972; Farago, 2008). Again, assuming paleosol trace-element concentrations are indicative of Permian soil-solution chemistries during glossopterid growth, the geochemistry of Wapadsberg Pass paleosols exhibits potentially stressed nutrient conditions. The concentration of Ni can be considered slightly elevated, and the concentrations of Cu, Ba, and Cr are high compared to modern soils that support healthy vegetation (see supplemental Tables DR4 and DR5 [see footnote 1]). Common abundances of these elements considered toxic in modern soils are on the order of 10 ppm for Cu and Ni, 1 ppm for Ba, and Cr in any small quantities (Hunt, 1972). Elevated amounts of Cu are mildly toxic, and Ba causes a decreased yield in plants by affecting and shutting down their stomatal openings (Hunt, 1972; Suwa et al., 2008), decreasing leaf size (Llugany et al., 2000), or both. Hence, small latest Changhsingian *Glossopteris* leaves may be a consequence of (1) soil chemistry; (2) tree maturity (e.g., juvenile plants), an interpretation that may be supported by the presence of thin, immature soils, although fully mature glossopterid forests are known to have grown on similar-thickness soils in Antarctica (Gulbranson et al., 2012); or (3) microphyllly characteristic of this particular taxon, morphotype W1 of Prevec et al. (2010).

### Implications of Stable Isotope Geochemical Trends

Tabor et al. (2007) used the carbon isotope values from OM (Ward et al., 2005) in conjunction with calcite  $\delta^{13}\text{C}$  values at the Carlton Heights Permian-Triassic boundary section to evaluate soil-drainage conditions at the time of calcite crystallization in the Karoo Basin. The carbon isotope data from OM (Ward et al., 2005) and paleosol calcite (Fig. 9) in Wapadsberg Pass can be used similarly to evaluate soil-drainage conditions in the latest Permian.

Calcite in well-drained soils is thought to form under open-system, one-dimensional, Fickian-type diffusive mixing of atmospheric CO<sub>2</sub> and CO<sub>2</sub> derived from in situ oxidation of soil OM (Cerling, 1991). Under these conditions, soil-formed calcite δ<sup>13</sup>C values will be more positive than coexisting OM δ<sup>13</sup>C values due to: (1) a 4.4‰ enrichment associated with diffusive transport of biologically derived CO<sub>2</sub> (Cerling, 1991); and (2) temperature-dependent carbon isotope enrichment associated with carbon isotope fractionation between carbonate species (Romanek et al., 1992):

$$\epsilon_{\text{cc-CO}_2}^{13} = 11.98 - 0.12 \times T (\text{°C}), \quad (3)$$

where  $\epsilon_{\text{cc-CO}_2}^{13}$  is an enrichment factor corresponding to the per mil difference between calcite and coexisting CO<sub>2</sub>.

Soil temperatures characteristically are warmer than mean annual surface temperatures (Buol et al., 1997), and carbonate isotopologue (Δ<sup>47</sup>) measurements of soil calcite indicate crystallization occurs at temperatures equivalent to the warm-season surface-air temperature (Passey et al., 2010; Quade et al., 2013). General circulation models of Permian paleogeography with NO-ICE scenarios (i.e., no substantial continental glacial ice) predict mean surface-air temperatures near 0 °C, with austral summer air temperatures of ~10 °C over this part of the Karoo Basin (Kiehl and Shields, 2005; Peyser and Poulsen, 2008). Hence, Late Permian, Karoo soil temperatures, when calcite crystallization occurred, are assumed to range between 15 and 25 °C. This temperature range translates to calcite δ<sup>13</sup>C values that will be at least 13.4‰ more positive than coexisting soil OM.

Ward et al. (2005) reported OM δ<sup>13</sup>C values ranging from -25.5‰ to -22.9‰ at Wapadsberg Pass, which is typical for Permian OM in the basin (Ward et al., 2005) and C3 photosynthesizers in general (O'Leary, 1981). Considering the relationship of carbon isotope fractionation

between OM and calcite, the range of paleosol calcite δ<sup>13</sup>C values that represents crystallization in equilibrium with CO<sub>2</sub> derived from OM oxidation in Wapadsberg Protosol carbonates is -12.1‰ to -8.2‰ (Fig. 9). Note that the δ<sup>13</sup>C values of C3 OM are 16‰–18‰ more negative than ambient atmospheric CO<sub>2</sub> (Arens et al., 2000). Therefore, the addition of any tropospheric CO<sub>2</sub> into the soil system during calcite crystallization only could result in more positive calcite δ<sup>13</sup>C values than those calculated only using the OM δ<sup>13</sup>C values (Fig. 9). This applies to calcite samples from paleosols between the stratigraphic heights of -60 m and -51 m in the Wapadsberg section (Table 1; Fig. 9). Furthermore, calcite δ<sup>13</sup>C values <-12.1‰ cannot be explained by Fickian-type, one-dimensional diffusive mixing of soil-derived CO<sub>2</sub> and atmospheric CO<sub>2</sub>. Rather, calcite in these paleosols likely formed under closed-system, poorly drained soil conditions (Tabor et al., 2007); this applies to samples taken from paleosols at 0 (vertebrate-defined Permian-Triassic boundary), -6, -18, -27, -33, -72, -76, -80.5, and -90 m in the section (Fig. 9). Calcite δ<sup>13</sup>C values between -12.1‰ and -8.3‰ may or may not have crystallized in soils characterized by one-dimensional CO<sub>2</sub> diffusion; this applies to samples originating from paleosols at -41, -45, and -65 m in the Wapadsberg Pass section.

Organic matter from acid-treated residues of samples 23606\_9, 23606\_8, and 23606\_23 have δ<sup>13</sup>C values of -26.1‰, -25.8‰, and -25.9‰, respectively (Table 2). These values are similar to carbon isotope values reported in previous studies of bulk OM δ<sup>13</sup>C values at several sites across the Permian-Triassic boundary (Ward et al., 2005), including Wapadsberg Pass (-25.5‰ to -22.9‰). Thus, calcite cements precipitated in poorly drained soils and sediment (Tabor et al., 2007) not only in siltstone and paleosol samples below the *Glossopteris* forest litter (-90 to -70 m; Prevec et al., 2010), but also in the interval leading up to, and includ-

ing, the highest carbonate nodule immediately below the end-Permian paleosol (DeKock and Kirschvink, 2004) and vertebrate-defined Permian-Triassic boundary. Values indicative of calcite cementation under well-drained conditions (Tabor et al., 2007) are restricted to the middle of the section (-60 to -40 m), with the most positive values associated with geometrically arrayed, small, spherical nodules precipitated around vertical roots at 60 m below the vertebrate-defined Permian-Triassic boundary (see Prevec et al., 2010, their figs. 3 and 4).

### Atmospheric pCO<sub>2</sub> Estimates

An estimate of atmospheric pCO<sub>2</sub> may be calculated using the δ<sup>13</sup>C values of coexisting paleosol calcite and OM in soils characterized by one-dimensional Fickian diffusive mixing of CO<sub>2</sub> according to the following two-end-member mixing equation:

$$C_{A(\text{cc})} = \frac{\delta^{13}\text{C}_{\text{cc}} - \delta^{13}\text{C}_{O(\text{cc})}}{\delta^{13}\text{C}_{A(\text{cc})} - \delta^{13}\text{C}_{O(\text{cc})}} * C_{S(\text{cc})} \quad (4)$$

Here, the subscript "cc" indicates calcite. The δ<sup>13</sup>C<sub>cc</sub> is the measured δ<sup>13</sup>C value of pedogenic calcite (δ<sup>13</sup>C<sub>CC</sub> in Tables 1 and 2). The δ<sup>13</sup>C values subscripted with "A" and "O" are predicted δ<sup>13</sup>C values of calcite if formed solely in equilibrium with CO<sub>2</sub> derived from the atmosphere and from oxidation of soil OM (i.e., respired CO<sub>2</sub>), respectively. C<sub>A</sub> refers to the concentration of CO<sub>2</sub> gas in the soil if the only contribution to soil CO<sub>2</sub> were from the atmosphere. C<sub>S</sub> is the actual concentration of CO<sub>2</sub> that was present in the soil at the time of calcite crystallization; it is the sum of atmospheric and soil-respired CO<sub>2</sub> (Yapp and Poths, 1996). Both C<sub>A</sub> and C<sub>S</sub> are in units of ppmV.

The δ<sup>13</sup>C<sub>O(cc)</sub> values may be estimated from δ<sup>13</sup>C values of coexisting OM in the soil profile (δ<sup>13</sup>C<sub>OM</sub> in Table 2). OM δ<sup>13</sup>C values from acid-

TABLE 2. ESTIMATES OF ATMOSPHERIC pCO<sub>2</sub>\*

Wapadsberg Pass sample number	Stratigraphic depth from PTB (m)	Petrographic texture	δ <sup>13</sup> C <sub>cc</sub> (‰)	δ <sup>13</sup> C <sub>OM</sub> (‰)	Atm pCO <sub>2</sub> low <sup>†</sup>	Atm pCO <sub>2</sub> high <sup>§</sup>
23606_9a	-41 m	Micrite	-10.7	-	900	1900
23606_9b	-41 m	Microspar	-9.3	-	800	1700
23606_9	-41 m	Organic matter from acid residue	-	-26.1	-	-
23606_8	-51 m	Gray microspar	-7.5	-	700	1500
23606_8	-51 m	Red microspar	-8	-	700	1500
23606_8	-51 m	Organic matter from acid residue	-	-25.8	-	-
23606_23	-60 m	Gray micrite rind	-5.5	-	500	1200
23606_23	-60 m	Gray with dendritic opaques	-6.2	-	600	1300
23606_23	-60 m	Microspar framboids	-5.3	-	500	1200
23606_23	-60 m	Organic matter from acid residue	-	-25.9	-	-

Note: PTB—vertebrate defined Permian-Triassic boundary; cc—calcite.

\*Based on calcite δ<sup>13</sup>C values of samples that either reflect almost certainly well-drained or possibly well-drained soils (see Fig. 9).

<sup>†</sup>pCO<sub>2</sub> estimates are based on C<sub>S</sub> values of 1000 ppmV; δ<sup>13</sup>C<sub>O</sub> values were calculated from an organic matter (OM) δ<sup>13</sup>C value at temperatures of 25 °C and δ<sup>13</sup>C<sub>A</sub> values of -8‰.

<sup>§</sup>pCO<sub>2</sub> estimates are based upon C<sub>S</sub> values of 2000 ppmV; δ<sup>13</sup>C<sub>O</sub> values were calculated from organic matter δ<sup>13</sup>C value at temperatures of 15 °C and δ<sup>13</sup>C<sub>A</sub> values of -5‰.

treated residues of paleosol-calcite nodules are  $-26.1\%$ ,  $-25.8\%$ , and  $-25.9\%$  for paleosols at  $-41$ ,  $-51$ , and  $-60$  m, respectively. The corresponding  $\delta^{13}\text{C}_{\text{O(occ)}}$  values for these samples include a  $4.4\%$  diffusive enrichment associated with oxidation of soil OM (Cerling, 1991), as well as a temperature-sensitive quantity of  $^{13}\text{C}$  enrichment associated with the phase transition from  $\text{CO}_2$  to calcite (Romanek et al., 1992):

$$\delta^{13}\text{C}_{\text{O(occ)}} = (\delta^{13}\text{C}_{\text{OM}} + 4.4\%) + \epsilon_{\text{cc-CO}_2}^{13}, \quad (5)$$

where  $\epsilon_{\text{cc-CO}_2}^{13}$  is equivalent to the quantity defined in Equation 2. The value of  $\delta^{13}\text{C}_A$  is calculated from the  $\delta^{13}\text{C}$  values of contemporaneous Upper Changhsingian marine calcites. Because marine calcite  $\delta^{13}\text{C}_A$  values range from  $\sim+3\%$  to  $0\%$  (Korte et al., 2004; Korte and Kozur, 2010), a corresponding range of  $\delta^{13}\text{C}_A$  values from  $-5\%$  to  $-8\%$  is used in calculations of  $p\text{CO}_2$  (Ekart et al., 1999). Calcite crystallization temperatures in Wapadsberg Pass Protosols are assumed to range between  $15^\circ\text{C}$  and  $25^\circ\text{C}$  and correspond to Late Permian soil temperatures in the Karoo Basin.

Values of  $C_s$  are unknown. However, studies of modern soils indicate that partial pressures of soil  $\text{CO}_2$  ( $C_s$ ) as well as soil-respired  $\text{CO}_2$  ( $S_z$ ) at the time of calcite crystallization can range from  $<1000$  to  $>10,000$  ppmV (Breecker et al., 2009; Mintz et al., 2011; Montañez, 2012; Tabor et al., 2013). For the kinds of paleosols that occur in the Karoo Basin (Calcsols), corresponding modern soils intimate soil-respired ( $S_z$ ) values of  $<1000$  ppmV (Breecker et al., 2009) to  $2000$  ppmV (Montañez, 2012). Therefore, we used  $C_s$  values ranging from  $1000$  to  $2000$  ppmV (note that in modern soils, these  $C_s$  values correspond to  $S_z$  values of  $\sim 600$ – $1600$  ppmV).

Coexisting calcite and OM  $\delta^{13}\text{C}$  values from paleosol profiles at  $-41$ ,  $-51$ , and  $-60$  m in the Wapadsberg Pass section provide a range of atmospheric  $p\text{CO}_2$  ( $C_{\text{A(occ)}}$ ) estimates from  $900$  to  $1900$ ,  $700$  to  $1700$ , and  $500$  to  $1300$  ppmV, respectively (Table 2). The assumed ranges of  $\delta^{13}\text{C}_O$ ,  $\delta^{13}\text{C}_A$ , and  $C_s$  result in significant uncertainty in estimates of Changhsingian atmospheric  $p\text{CO}_2$ . In spite of these large uncertainties, the current data provide persuasive evidence that Changhsingian atmospheric  $p\text{CO}_2$  was substantially higher (at least  $\sim 2\times$  higher) than modern, pre-industrial atmospheric  $p\text{CO}_2$  ( $\sim 280$  ppmV; Petit et al., 1999). However, the lower range of these atmospheric  $p\text{CO}_2$  estimates is well within the envelope of atmospheric  $p\text{CO}_2$  that is predicted for A.D. 2100 in a “business as usual” Intergovernmental Panel on Climate Change scenario (Solomon et al., 2007), and it is consistent with estimates by Brand et al. (2010) based on brachiopods from the southern Alps.

## CONCLUSIONS

Geochemical trends in late Changhsingian paleosols,  $\sim 70$  m below the vertebrate-defined Permian-Triassic boundary at Wapadsberg Pass (Ward et al., 2000, 2005), Eastern Cape Province, South Africa, indicate the presence of wetland Protosols coincident with autochthonous *Glossopteris* forest litters as reported by Prevec et al. (2010). Paleosol profile trends in TOC, base loss (Na, Ca, K, Mg/Ti), clayeyness (Al/Si), mineral assemblage stability (Fe/K), calcification ( $[\text{Ca} + \text{Mg}]/\text{Al}$ ), salinization ( $[\text{K} + \text{Na}]/\text{Al}$ ), and mineral maturity (Si/Al) support the interpretation of two stacked, aggradational, and poorly developed paleosols. These were immature landscapes, formed under a warm and wet climate, as evidenced by average CIA–K values of  $77$ ; CIA–K values are similar to those reported for paleosols formed during the deglaciation transition into the Middle Permian (Scheffler et al., 2003, 2006). Major- and trace-element abundances in Wapadsberg Pass Protosols are similar to values reported by Coney et al. (2007) for the uppermost  $\sim 7$  m of the Elandsberg Member (Changhsingian) and lower  $2+$  m of the Palingkloof Member (Induan) at Old Wapadsberg Pass, where little variation in elemental abundance occurs across the vertebrate-defined Permian-Triassic boundary. Coney et al. (2007) attributed all geochemical variation to changes in lithology rather than responses to a change in climate. Major- and trace-element values in the New Wapadsberg Pass Protosols indicate that similar chemistries also prevailed lower in the preboundary section. Making the assumption that pre- and post-boundary siltstones analyzed by Coney et al. (2007) represent floodplain paleosols, following previous interpretations (Smith and Ward, 2001; Ward et al., 2000, 2005; Retallack et al., 2003; De Kock and Kirschvink, 2004), average CIA–K values of  $60$  and  $70$  are found for the uppermost Permian and lowermost Triassic, respectively. CIA–K values, alone, may be indicative of a trend toward stronger, more pronounced seasonality in the sediments bounding the vertebrate-defined Permian-Triassic boundary in this part of the Karoo Basin.

In contrast, the  $\delta^{13}\text{C}$  trend identified from analysis of micrite and microspar cements of carbonate nodules throughout the  $90+$  m Wapadsberg section indicates that only one stratigraphic interval is characterized by calcite precipitated under well-drained soil conditions. This interval is not coincident with the vertebrate-defined Permian-Triassic boundary; rather, it occurs  $\sim 60$  m below the stratigraphic level at which the boundary has been placed by others (e.g., Ward et al., 2000, 2005). Most  $\delta^{13}\text{C}$  values reflect cal-

cite precipitation under saturated sediment conditions, a finding more parsimonious with the known wetland habit of the glossopterids (Greb et al., 2006), remains of which are preserved to within  $6$  m of the reported boundary (Gastaldo et al., 2005). Hence, no unidirectional aridification trend is identified in calcite cements of calcareous nodules in this Permian-Triassic boundary section; rather, paleosol nodules up to the end-Permian paleosol (DeKock and Kirschvink, 2004) formed in saturated soils or sediments.

We present the first estimates of latest Permian atmospheric  $p\text{CO}_2$  from paleosols based on coexisting calcite and OM  $\delta^{13}\text{C}$  values in the Wapadsberg Pass section, where calcite precipitated in both possibly well-drained and almost certainly well-drained conditions. Latest Changhsingian atmospheric  $p\text{CO}_2$  estimates from three paleosols at  $-41$  m,  $-51$  m, and  $-60$  m below the vertebrate-defined Permian-Triassic boundary at this locality range from  $900$  to  $1900$ ,  $700$  to  $1700$ , and  $500$  to  $1300$  ppmV, respectively. These are significantly lower than terrestrial-based Early Permian estimates for global deglaciation provided by Montañez et al. (2007), which are as high as  $3500$  ppmV at the beginning of the Kungurian, when a shift in vegetational biomes is recognized. Hence, atmospheric  $p\text{CO}_2$  estimates prior to the end Paleozoic event, as defined by vertebrate biostratigraphy (Ward et al., 2005), are consistent with estimates from marine brachiopods (Brand et al., 2012) but are not as extreme as those envisioned during global deglaciation pulses earlier in the Permian.

## ACKNOWLEDGMENTS

We acknowledge the field assistance of Rose Prevec (Rhodes University), Sandra Kamo (University of Toronto), Cindy Looy (University of California–Berkeley), and Samuel Reid and Amelia Pludow (Colby College). Appreciation is extended to the following colleagues for assistance with laboratory analyses: V. Reynolds and E. Crapster-Pregont, Colby College (inductively coupled plasma–optical emission spectrometry); B.F. Rueger and D.B. Allen, Colby College (X-ray diffraction) analyses; and D. Gibson, University of Maine–Farmington (X-ray fluorescence). Nathan Sheldon and an anonymous reviewer are thanked for their critical reading of the manuscript and suggestions to improve its content. Project support included funding from the Sullivan–Garner Fund grant and Claire-Booth-Luce funds, Colby College; National Science Foundation grants EAR-0417317 and EAR-1123570; and sabbatical support from the Alexander von Humboldt Stiftung, Bonn, Germany, and a Fulbright Fellowship at Rhodes University, Grahamstown, South Africa, to Gastaldo.

## REFERENCES CITED

- Aitkinhead, J.A., and McDowell, W.L.I., 2000, Soil C:N ratio as a predictor of annual riverine DOC flux at local and global scales: Global Biogeochemical Cycles, v. 14, p. 127–138, doi:10.1029/1999GB900083.

- Arens, N.A., Jahren, A.H., and Amundson, R., 2000, Can C3 plants faithfully record the carbon isotopic composition of atmospheric carbon dioxide?: *Paleobiology*, v. 26, p. 137–164.
- Bordy, E.M., Segwabe, T., and Makuke, B., 2010, Sedimentology of the Upper Triassic–Lower Jurassic (?) Mosolotsane Formation (Karoo Supergroup), Kalahari Karoo Basin, Botswana: *Journal of African Earth Sciences*, v. 58, p. 127–140, doi:10.1016/j.jafrearsci.2010.02.006.
- Bordy, E.M., Sztanó, O., Rubidge, B.S., and Bumby, A., 2011, Early Triassic vertebrate burrows from the Katberg Formation of the south-western Karoo Basin, South Africa: *Lethaia*, v. 44, p. 33–45, doi:10.1111/j.1502-3931.2010.00223.x.
- Botha, J., and Smith, R.M.H., 2006, Rapid vertebrate recuperation in the Karoo Basin of South Africa following the end-Permian extinction: *Journal of African Earth Sciences*, v. 45, p. 502–514, doi:10.1016/j.jafrearsci.2006.04.006.
- Botha, J., and Smith, R.M.H., 2007, *Lystrosaurus* species composition across the Permo–Triassic boundary in the Karoo Basin of South Africa: *Lethaia*, v. 40, p. 125–137, doi:10.1111/j.1502-3931.2007.00011.x.
- Boutton, T.W., 1991, Stable carbon isotope ratios of natural materials: II. Atmospheric, terrestrial, marine, and freshwater environments, in Coleman, D.C., and Fry, B., eds., *Carbon Isotope Techniques*: San Diego, California, Academic Press, p. 173–186.
- Brand, U., Posenato, R., Came, R., Affek, H., Angiolini, L., Azmy, K., and Farabegoli, E., 2010, The end-Permian mass extinction: A rapid volcanic CO<sub>2</sub> and CH<sub>4</sub>-climatic catastrophe: *Chemical Geology*, v. 322–323, p. 121–144.
- Breecker, D.O., Sharp, Z.D., and McFadden, L.D., 2009, Seasonal bias in the formation and stable isotopic composition of pedogenic carbonate in modern soils from central New Mexico, U.S.A.: *Geological Society of America Bulletin*, v. 121, p. 630–640, doi:10.1130/B26413.1.
- Bull, W.B., 1991, *Geomorphic Responses to Climate Change*: New York, Oxford University Press, 326 p.
- Buol, S.W., Hole, F.D., McCracken, R.J., and Southard, R.J., 1997, *Soil Genesis and Classification* (4th ed.): Ames, Iowa, Iowa State University Press, 494 p.
- Burt, R., Wilson, M.A., Mays, M.D., and Lee, C.W., 2003, Major and trace elements of selected pedons in the USA: *Journal of Environmental Quality*, v. 32, p. 2109–2121, doi:10.2134/jeq2003.2109.
- Caudill, M.R., Driese, S.G., and Mora, C.I., 1996, Preservation of a paleo-Vertisol and an estimate of late Mississippian paleoprecipitation: *Journal of Sedimentary Research*, v. 66, p. 58–70.
- Cerling, T.E., 1991, Carbon dioxide in the atmosphere: Evidence from Cenozoic and Mesozoic paleosols: *American Journal of Science*, v. 291, p. 377–400, doi:10.2475/ajs.291.4.377.
- Coney, L., 2005, Mineralogical–Geochemical Investigation of Two Sections Across the Permian–Triassic Boundary in the Continental Realm of the Southern Karoo Basin, South Africa [M.Sc. thesis]: Johannesburg, South Africa, University of the Witwatersrand, 177 p.
- Coney, L., Reimold, W.U., Hancox, J.P., Mader, D., Koeberl, C., McDonald, L., Stuck, U., Vajda, V., and Kamo, S.L., 2007, Geochemical and mineralogical investigation of the Permian–Triassic boundary in the continental realm of the southern Karoo Basin, South Africa: *Paleoworld*, v. 16, p. 67–104, doi:10.1016/j.palwor.2007.05.003.
- Craig, H., 1957, Isotopic standards for carbon and oxygen and correction factors for mass spectrometric analysis of carbon dioxide: *Geochimica et Cosmochimica Acta*, v. 12, p. 133–149, doi:10.1016/0016-7037(57)90024-8.
- De Kock, M.O., and Kirschvink, J.L., 2004, Paleomagnetic constraints on the Permian–Triassic boundary in terrestrial strata of the Karoo Supergroup, South Africa: Implications for causes of the end-Permian extinction event: *Gondwana Research*, v. 7, p. 175–183, doi:10.1016/S1342-937X(05)70316-6.
- De Wit, M.J., Ghosh, J.G., De Villiers, S., Rakotosolof, N., Alexander, J., Tripathi, A., and Looy, C., 2002, Multiple organic carbon isotope reversals across the Permian–Triassic boundary of terrestrial Gondwanan sequences: Clues to extinction patterns and delayed ecosystem recovery: *The Journal of Geology*, v. 110, p. 227–240, doi:10.1086/338411.
- DiMichele, W.A., and Gastaldo, R.A., 2008, Plant paleoecology in deep time: *Annals of the Missouri Botanical Garden*, v. 95, p. 144–198, doi:10.3417/2007016.
- Ekart, D.D., Cerling, T.E., Montañez, I.P., and Tabor, N.J., 1999, A 400 million year carbon isotope record of pedogenic carbonate: Implications for paleoatmospheric carbon dioxide: *American Journal of Science*, v. 299, p. 805–827, doi:10.2475/ajs.299.10.805.
- Farago, M.E., ed., 2008, *Plants and the Chemical Elements*: New York, J.W. Wiley, E-book, 302 p.
- Gastaldo, R.A., and Demko, T.M., 2010, Long term hydrology controls the plant fossil record, in Allison, P.A., and Bottjer, D.J., eds., *Taphonomy: Processes and Bias Through Time* (2nd ed.): Topics in Geobiology, v. 32, p. 249–286, doi:10.1007/978-90-481-8643-3\_7.
- Gastaldo, R.A., and Neveling, J., 2012, The terrestrial Permian–Triassic boundary event is a nonevent: Reply: *Geology*, v. 40, p. e257, doi:10.1130/G32975Y.1.
- Gastaldo, R.A., Adendorff, R., Bamford, M., Labandeira, C.C., Neveling, J., and Sims, H., 2005, Taphonomic trends of macrofloral assemblages across the Permian–Triassic boundary, Karoo Basin, South Africa: *Palaio*, v. 20, p. 479–497, doi:10.2110/palo.2004.P04-62.
- Gastaldo, R.A., Neveling, J., Clark, C.K., and Newbury, S.S., 2009, The terrestrial Permian–Triassic boundary event bed is a non-event: *Geology*, v. 37, p. 199–202, doi:10.1130/G25255A.1.
- Gladney, E.S., and Roelands, I., 1988, 1987 Compilation of elemental concentration data for USGS BIR-1, DNC-1, and W-2: *Geostandards Newsletter*, v. 12, p. 63–118, doi:10.1111/j.1751-908X.1988.tb00044.x.
- Greb, S.F., DiMichele, W.D., and Gastaldo, R.A., 2006, Evolution of wetland types and the importance of wetlands in Earth history, in DiMichele, W.A., and Greb, S., eds., *Wetlands Through Time*: Geological Society of America Special Paper 399, p. 1–40, doi:10.1130/2006.2399(01).
- Gulbranson, E.L., Isbell, J.L., Taylor, E.L., Ryberg, P.E., Taylor, T.N., and Flaig, P.P., 2012, Permian polar forests: Deciduous and environmental variation: *Geobiology*, v. 10, p. 479–495, doi:10.1111/j.1472-4669.2012.00338.x.
- Hancox, J.P., Brandt, D., Reimold, W.U., Koeberl, C., and Neveling, J., 2002, Permian–Triassic boundary in the Northwest Karoo Basin: Current stratigraphic placement, implications for basin development models, and search for evidence of impact, in Koeberl, C., and MacLeod, K.G., eds., *Catastrophic Events and Mass Extinctions: Impacts and Beyond*: Geological Society of America Special Paper 356, p. 429–444, doi:10.1130/0-8137-2356-6.429.
- Hunt, C.B., 1972, *Geology of Soils: Their Evolution, Classification, and Uses*: New York, W.H. Freeman and Company, 344 p.
- Kammerer, C.F., Angielczyk, K.D., and Fröbisch, J., 2011, A comprehensive taxonomic revision of *Dicynodon* (Therapsida, Anomodontia) and its implications for dicynodont phylogeny, biogeography, and biostratigraphy: *Journal of Vertebrate Paleontology*, v. 31, supplement 1, p. 1–158, doi:10.1080/02724634.2011.627074.
- Kiehl, J.T., and Shields, C.A., 2005, Climate simulation of the latest Permian: Implications for mass extinction: *Geology*, v. 33, p. 757–760, doi:10.1130/G21654.1.
- Korte, C., and Kozur, H.W., 2010, Carbon isotope stratigraphy across the Permian–Triassic boundary: A review: *Journal of Asian Earth Sciences*, v. 39, p. 215–235, doi:10.1016/j.jseaes.2010.01.005.
- Korte, C., Kozur, H.W., Joachimski, M.M., Strauss, H., Veizer, J., and Schwark, L., 2004, Carbon, sulfur, oxygen and strontium isotope records, organic geochemistry and biostratigraphy across the Permian–Triassic boundary in Abadeh, Iran: *International Journal of Earth Sciences*, v. 93, p. 565–581.
- Lugany, M., Poschenrieder, C., and Barceló, J., 2000, Assessment of barium toxicity in bush beans: *Archives of Environmental Contamination and Toxicology*, v. 39, p. 440–444, doi:10.1007/s002440010125.
- Lynn, W.C., Ahrens, R.J., and Smith, A.L., 2002, Soil minerals, their geographic distribution, and soil taxonomy, in Amonette, J.E., Bleam, W.F., Schulze, D.G., and Dixon, J.B., eds., *Soil Mineralogy with Environmental Applications*: Madison, Wisconsin, Soil Science Society of America, Book Series 7, p. 691–709.
- Mack, G.H., James, W.C., and Monger, H.C., 1993, Classification of paleosols: *Geological Society of America Bulletin*, v. 105, p. 129–136, doi:10.1130/0016-7606(1993)105<0129:COP>2.3.CO;2.
- MacLeod, K.G., Smith, R.M.H., Koch, P.L., and Ward, P.D., 2000, Timing of mammal-like reptile extinctions across the Permian–Triassic boundary in South Africa: *Geology*, v. 28, p. 227–230, doi:10.1130/0091-7613(2000)28<227:TOMREA>2.0.CO;2.
- Maruoka, T., Koeberl, C., Hancox, J.P., and Reimold, W.U., 2003, Sulfur geochemistry across a terrestrial Permian–Triassic boundary section in the Karoo Basin, South Africa: *Earth and Planetary Science Letters*, v. 206, p. 101–117, doi:10.1016/S0012-821X(02)01087-7.
- Maynard, J.B., 1992, Chemical of modern soils as a guide to interpreting Precambrian paleosols: *The Journal of Geology*, v. 100, p. 279–289, doi:10.1086/629632.
- McCrea, J.M., 1950, On the isotopic chemistry of carbonates and a paleotemperature scale: *The Journal of Chemical Physics*, v. 18, p. 849–857, doi:10.1063/1.1747785.
- Meyers, P.A., 1994, Preservation of elemental and isotopic source identification of sedimentary organic matter: *Chemical Geology*, v. 114, p. T289–T302, doi:10.1016/0009-2541(94)90059-0.
- Mintz, J.S., Driese, S.G., Breecker, D.O., and Ludvigson, G.A., 2011, Influence of changing hydrology on pedogenic calcite precipitation in Vertisols, Dance Bayou, Brazoria County, TX: Implications for estimating paleoatmospheric pCO<sub>2</sub>: *Journal of Sedimentary Research*, p. 394–400, doi:10.2110/jrsr.2011.36.
- Montañez, I.P., 2012, Modern soil system constraints on reconstructing deep-time atmospheric CO<sub>2</sub>: *Geochimica et Cosmochimica Acta*, v. 101, p. 57–75, doi:10.1016/j.gca.2012.10.012.
- Montañez, I.P., Tabor, N.J., Niemeier, D., DiMichele, W.A., Frank, T.D., Fielding, C.R., Isbell, J.L., Birgenheier, L.P., and Rygel, M.C., 2007, CO<sub>2</sub>-forced climate instability and linkages to tropical vegetation during late Paleozoic deglaciation: *Science*, v. 315, p. 87–91, doi:10.1126/science.1134207.
- Nesbitt, W., and Young, G.M., 1982, Early Proterozoic climates and plate motions inferred from major element chemistry of lutites: *Nature*, v. 299, p. 715–717, doi:10.1038/299715a0.
- O’Leary, M.H., 1981, Carbon isotope fractionation in plants: *Phytochemistry*, v. 20, p. 553–567, doi:10.1016/0031-9422(81)85134-5.
- Passey, B.H., Levin, N.E., Cerling, T.E., Brown, F.H., and Eiler, J.M., 2010, High-temperature environments of human evolution in East Africa based on bond ordering in paleosol carbonates: *Proceedings of the National Academies of Sciences of the United States of America*, v. 107, p. 11,245–11,249, doi:10.1073/pnas.1001824107.
- Payne, J.L., and Clapham, M.E., 2012, End-Permian mass extinction in the oceans: An ancient analog for the twenty-first century: *Annual Reviews of Earth and Planetary Science Letters*, v. 40, p. 89–111, doi:10.1146/annurev-earth-042711-105329.
- Petit, J.R., Jouzel, J., Raynaud, D., Barkov, N.I., Barnola, J.-M., Basile, I., Chappellaz, J., Davis, M., Delaygue, G., Delmotte, M., Kotlyakov, V.M., Legrand, M., Lipenkov, V.Y., Lorius, C., Papin, L., Ritz, C., Saltzman, E., and Stevenard, M., 1999, Climate and atmospheric history of the past 420,000 years from the Vostok ice core, Antarctica: *Nature*, v. 399, p. 429–436, doi:10.1038/20859.
- Peyser, C.E., and Poulsen, C.J., 2008, Controls on Permo-Carboniferous precipitation over tropical Pangaea: A GCM sensitivity study: *Palaogeography, Palaeoclimatology, Palaeoecology*, v. 268, p. 181–192, doi:10.1016/j.palaeo.2008.03.048.
- Pollastro, R.M., 1982, A Recommended Procedure for the Preparation of Clay Mineral Specimens for X-Ray Diffraction Analysis—Modifications to Drever’s Filter-Membrane Peel Technique: *U.S. Geological Survey Open-File Report 82-71*, 10 p.
- Prevec, R., Gastaldo, R.A., Neveling, J., Reid, S.B., and Looy, C.V., 2010, An autochthonous Glossopterid flora

- with latest Permian palynomorphs from the *Dicynodon* assemblage zone of the southern Karoo Basin, South Africa: *Palaeogeography, Palaeoclimatology, Palaeoecology*, v. 292, p. 391–408, doi:10.1016/j.palaeo.2010.03.052.
- Quade, J., Eiler, J., Daëron, M., and Achyuthan, H., 2013, The clumped isotope geothermometer in soil and paleosol carbonate: *Geochimica et Cosmochimica Acta*, v. 105, p. 92–107, doi:10.1016/j.gca.2012.11.031.
- Reid, S.B., Gastaldo, R.A., Neveling, J., and Tabor, N., 2007, Fluvial systems and carbonate nodules reveal Late Permian climate change at Wapadsberg Pass, Eastern Cape Province, South Africa: *Geological Society of America Abstracts with Program*, v. 39, no. 6, p. 85.
- Retallack, G.J., 2002, *Lepidopteris callipteroides*, an earliest Triassic seed fern of the Sydney Basin, southeastern Australia: *Alcheringa*, v. 26, p. 475–500, doi:10.1080/03115510208619538.
- Retallack, G.J., Smith, R.M.H., and Ward, P.D., 2003, Vertebrate extinction across Permian-Triassic boundary in Karoo Basin, South Africa: *Geological Society of America Bulletin*, v. 115, p. 1133–1152, doi:10.1130/B25215.1.
- Romanek, C.S., Grossman, E.L., and Morse, J.W., 1992, Carbon isotopic fractionation in synthetic aragonite and calcite: Effects of temperature and precipitation rate: *Geochimica et Cosmochimica Acta*, v. 56, p. 419–430, doi:10.1016/0016-7037(92)90142-6.
- Rubidge, B.S., ed., 1995, *Biostratigraphy of the Beaufort Group (Karoo Supergroup)*: Geological Survey of South Africa *Biostratigraphic Series 1*, p. 1–46.
- Scheffler, K., Hoernes, S., and Schwark, L., 2003, Global changes during Carboniferous-Permian glaciation of Gondwana: Linking polar and equatorial climate evolution by geochemical proxies: *Geology*, v. 31, p. 605–608, doi:10.1130/0091-7613(2003)031<0605:GCDCGO>2.0.CO;2.
- Scheffler, K., Buehmann, D., and Schwark, L., 2006, Analysis of late Palaeozoic glacial to postglacial sedimentary successions in South Africa by geochemical proxies—Response to climate evolution and sedimentary environment: *Palaeogeography, Palaeoclimatology, Palaeoecology*, v. 6, p. 184–203.
- Sheldon, N.D., 2005, Do red beds indicate paleoclimatic conditions?: A Permian case study: *Palaeogeography, Palaeoclimatology, Palaeoecology*, v. 228, p. 305–319, doi:10.1016/j.palaeo.2005.06.009.
- Sheldon, N.D., and Tabor, N.J., 2009, Quantitative paleoenvironmental and paleoclimatic reconstruction using paleosols: *Earth-Science Reviews*, v. 95, p. 1–52, doi:10.1016/j.earscirev.2009.03.004.
- Sheldon, N.D., Retallack, G.J., and Tanaka, S., 2002, Geochemical climofunctions from North America soils and application to paleosols across the Eocene-Oligocene boundary in Oregon: *The Journal of Geology*, v. 110, p. 687–696, doi:10.1086/342865.
- Shen, S.Z., Crowley, J.L., Wang, Y., Bowring, S.A., Erwin, D.H., Sadler, P.M., Cao, C.Q., Rothman, D.H., Henderson, C.M., Ramezani, J., Zhang, H., Shen, Y., Wang, X.D., Wang, W., Mu, L., Li, W.Z., Tang, Y.G., Liu, X.L., Liu, L.J., Zeng, Y., Jiang, Y.F., and Jin, Y.G., 2011, Calibrating the end-Permian mass extinction: *Science*, v. 334, p. 1367–1372, doi:10.1126/science.1213454.
- Smith, R.M.H., 1995, Changing fluvial environments across the Permian-Triassic boundary in the Karoo Basin, South Africa, and possible causes of tetrapod extinctions: *Palaeogeography, Palaeoclimatology, Palaeoecology*, v. 117, p. 81–104, doi:10.1016/0031-0182(94)00119-S.
- Smith, R.M.H., and Botha, J., 2005, The recovery of terrestrial vertebrate diversity in the South African Karoo Basin after the end-Permian extinction: *Comptes Rendus, Palévol*, v. 4, p. 555–568.
- Smith, R.M.H., and Ward, P.D., 2001, Pattern of vertebrate extinctions across an event bed at the Permian-Triassic boundary in the Karoo Basin of South Africa: *Geology*, v. 29, p. 1147–1150, doi:10.1130/0091-7613(2001)029<1147:POVEAA>2.0.CO;2.
- Solomon, S., Qin, D., Manning, M., Chen, Z., Marquis, M., Averyt, K.B., Tignor, M., and Miller, H.L., eds., 2007, *Climate Change 2007: The Physical Science Basis: Contribution of Working Group I to the Fourth Assessment Report of the Intergovernmental Panel on Climate Change*: Cambridge, UK, Cambridge University Press, 996 p.
- Stollhofen, H., Werner, M., Stanistreet, I.G., and Armstrong, R.A., 2008, Single-zircon U-Pb dating of Carboniferous-Permian tuffs, Namibia, and the intercontinental deglaciation cycle framework, *in* Fielding, C.R., Frank, T.D., and Isbell, J.L., eds., *Resolving the Late Paleozoic Ice Age in Time and Space*: Geological Society of America Special Paper 441, p. 83–96, doi:10.1130/2008.2441(06).
- Suwa, R., Jayachandran, K., Nguyen, N.T., Boulouvar, A., Fujita, K., and Saneoka, H., 2008, Barium toxicity effects in soybean plants: *Archives of Environmental Contamination and Toxicology*, v. 55, p. 397–403, doi:10.1007/s00244-008-9132-7.
- Tabor, N.J., Montañez, I.P., Steiner, M.B., and Schwindt, D., 2007, <sup>13</sup>C values of carbonate nodules across the Permian-Triassic boundary in the Karoo Supergroup (South Africa) reflect a stinking sulfurous swamp, not atmospheric CO<sub>2</sub>: *Palaeogeography, Palaeoclimatology, Palaeoecology*, v. 252, p. 370–381, doi:10.1016/j.palaeo.2006.11.047.
- Tabor, N.J., Myers, T.S., Gulbranson, E., Rasmussen, C., and Sheldon, N.D., 2013, Carbon isotope composition of marine and terrestrial ecosystems during the end-Permian biotic crisis: *Geology*, v. 29, p. 351–354, doi:10.1130/0091-7613(2001)029<0351:RASCOM>2.0.CO;2.
- Twitchett, R.J., Looy, C.V., Morante, R., Visscher, H., and Wignall, P.B., 2001, Rapid and synchronous collapse of marine and terrestrial ecosystems during the end-Permian biotic crisis: *Geology*, v. 29, p. 351–354, doi:10.1130/0091-7613(2001)029<0351:RASCOM>2.0.CO;2.
- Vyzamal, J., 1995, *Algae and Element Cycling in Wetlands*: Chicago, Illinois, Lewis Publishers, 689 p.
- Ward, P.D., Montgomery, D.R., and Smith, R.M.H., 2000, Altered river morphology in South Africa related to the Permian-Triassic extinction: *Science*, v. 289, p. 1740–1743, doi:10.1126/science.289.5485.1740.
- Ward, P.D., Botha, J., Buick, R., DeKock, M.O., Erwin, D.H., Garrison, G., Kirschvink, J., and Smith, R.M.H., 2005, Abrupt and gradual extinction among Late Permian land vertebrates in the Karoo Basin, South Africa: *Science*, v. 307, p. 709–714, doi:10.1126/science.1107068.
- Xiong, C., and Wang, Q., 2011, Permian-Triassic land-plant diversity in South China: Was there a mass extinction at the Permian/Triassic boundary?: *Paleobiology*, v. 37, p. 157–167, doi:10.1666/09029.1.
- Yapp, C.J., and Poths, H., 1996, Carbon isotopes in continental weathering environments and variations in ancient atmospheric CO<sub>2</sub> pressure: *Earth Planetary Science Letters*, v. 137, p. 71–82.

SCIENCE EDITOR: CHRISTIAN KOEBERL

ASSOCIATE EDITOR: TROY RASBURY

MANUSCRIPT RECEIVED 19 MARCH 2013

REVISED MANUSCRIPT RECEIVED 6 AUGUST 2013

MANUSCRIPT ACCEPTED 26 NOVEMBER 2013

Printed in the USA